CALORIMETRY

Energy measurement in Particle Physics

Richard WIGMANS

(Texas Tech University)

ICFA Instrumentation School, Istanbul

August 27 - September 10, 2005

CALORIMETRY

Energy Measurement in Particle Physics

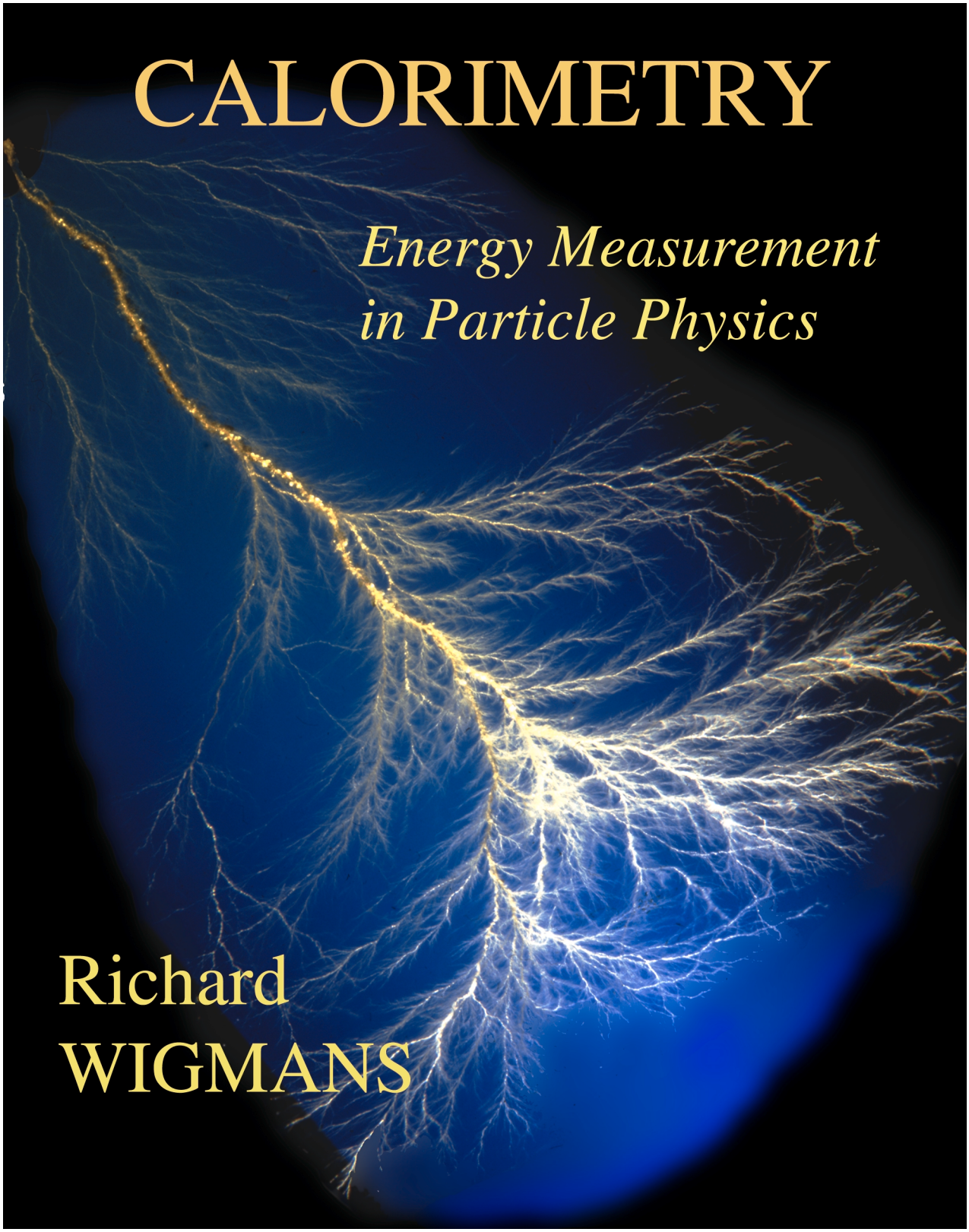

Richard WIGMANS

INTRODUCTION

- Calorimeters most important detectors in many modern experiments
  Sometimes the *only* detectors (SuperK, Icarus, Amanda, Auger,....)

  - *Provide* ***unique information***
    (neutral particles, jets, missing E_T, particle ID,.....)

  - *Information becomes* ***more precise as energy increases***
    (contrary to tracking systems)

  - ***Triggering capability*** *in complex environment*
    (fast signals, clever logic)

  - *Miscellaneous properties*
    (absorber for μ detection, return yoke for magnetic flux)

- Important calorimeter properties:

  - *Energy* ***resolution*** but also
  - *Signal* ***speed***
  - *Correct energy scale (****linearity****)*
  - ***Particle ID*** *capability (granularity)*

The importance of energy resolution (electromagnetic)

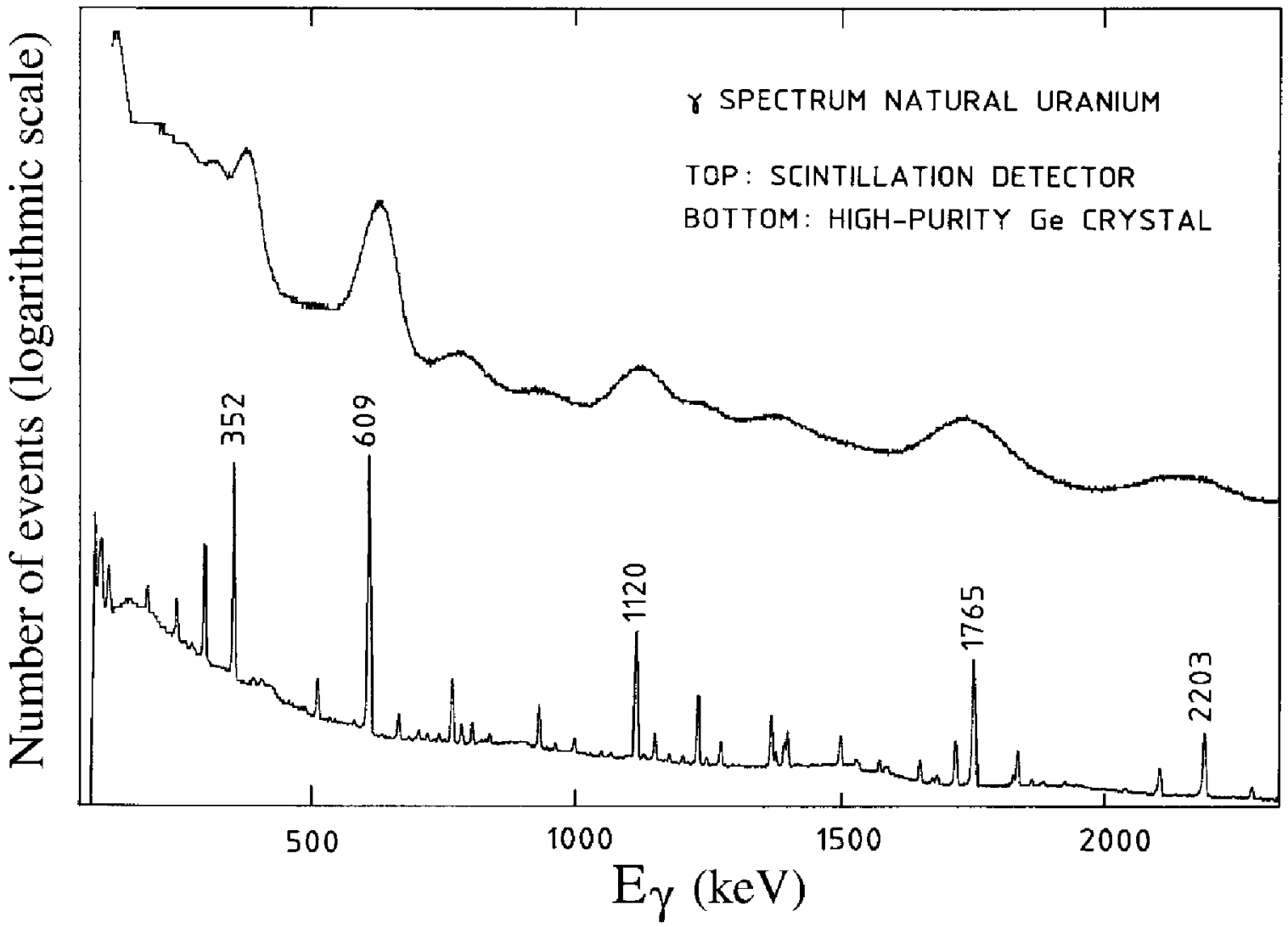

FIG. 1.1. Nuclear γ-ray spectrum of decaying uranium nuclei, measured with a bismuth germaniumoxide scintillation counter (*upper curve*) and with a high-purity germanium crystal (*lower curve*). Courtesy of G. Roubaud, CERN.

The importance of energy resolution (hadronic)

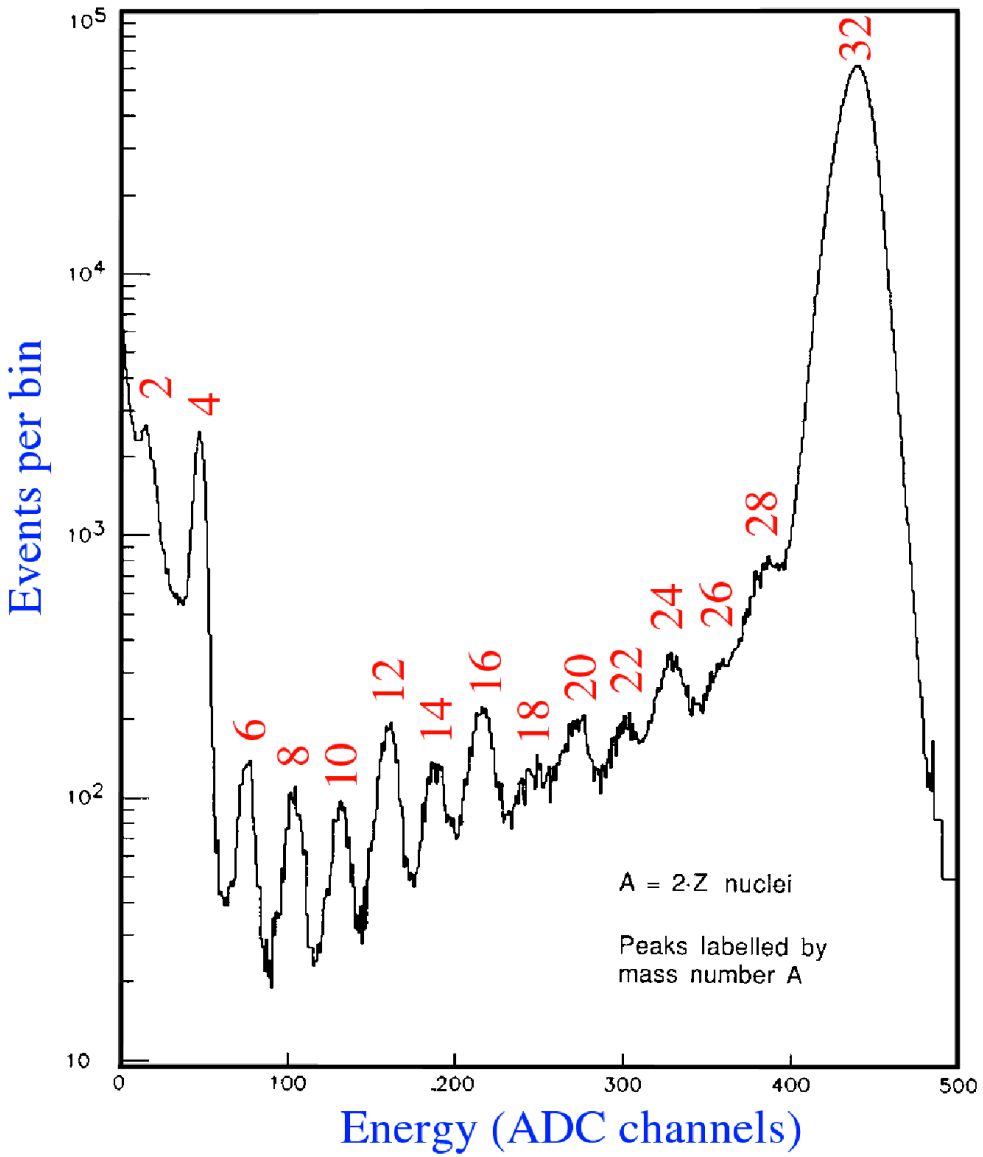

FIG. 7.51. The WA80 calorimeter as a high-resolution spectrometer. Total energy measured with the calorimeter for minimum-bias events revealed the composition of the momentum-selected CERN heavy-ion beam [You 89].

The importance of energy resolution

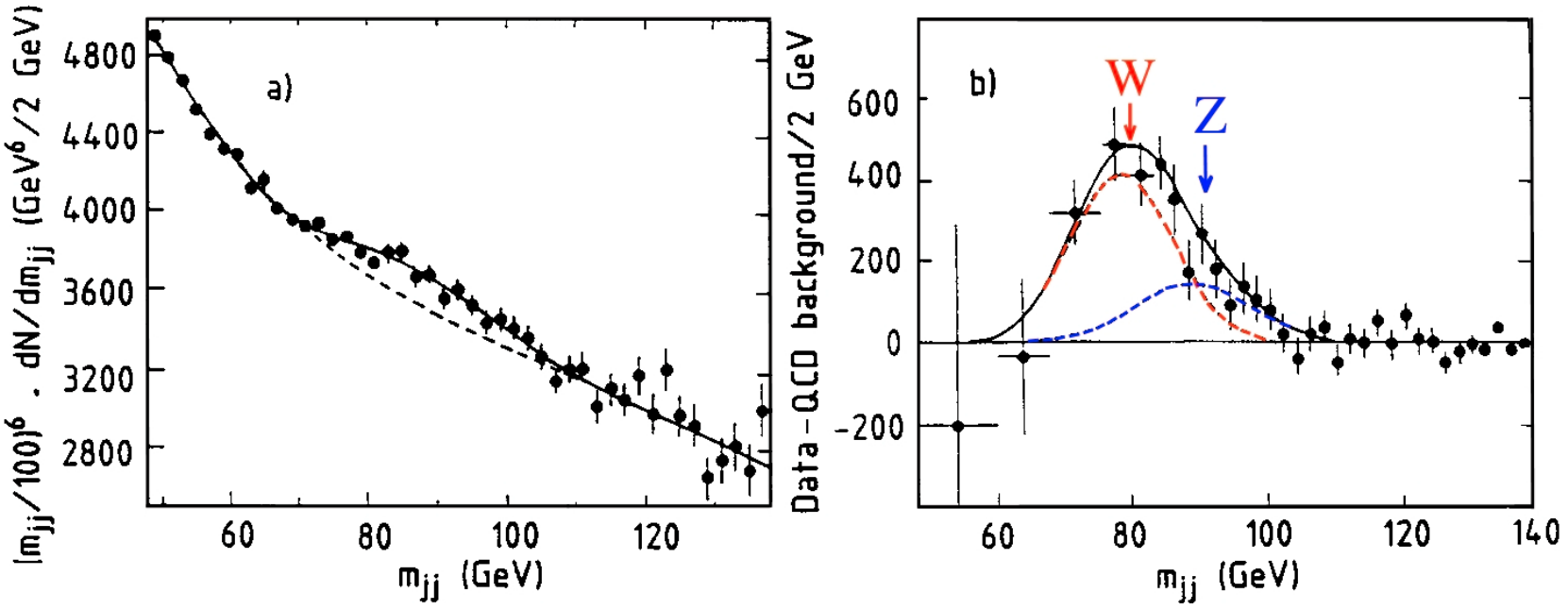

FIG. 7.50. Two-jet invariant mass distributions from the UA2 experiment [Alit 91]. Diagram a) shows the measured data points, together with the results of the best fits to the QCD background alone (*dashed curve*), or including the sum of two Gaussian functions describing $W, Z \to q\bar{q}$ decays. Diagram b) shows the same data after subtracting the QCD background. The data are compatible with peaks at $m_W = 80$ GeV and $m_Z = 90$ GeV. The measured width of the bump, or rather the standard deviation of the mass distribution, was 8 GeV, of which 5 GeV could be attributed to non-ideal calorimeter performance [Jen 88].

Signal speed of Čerenkov calorimeters

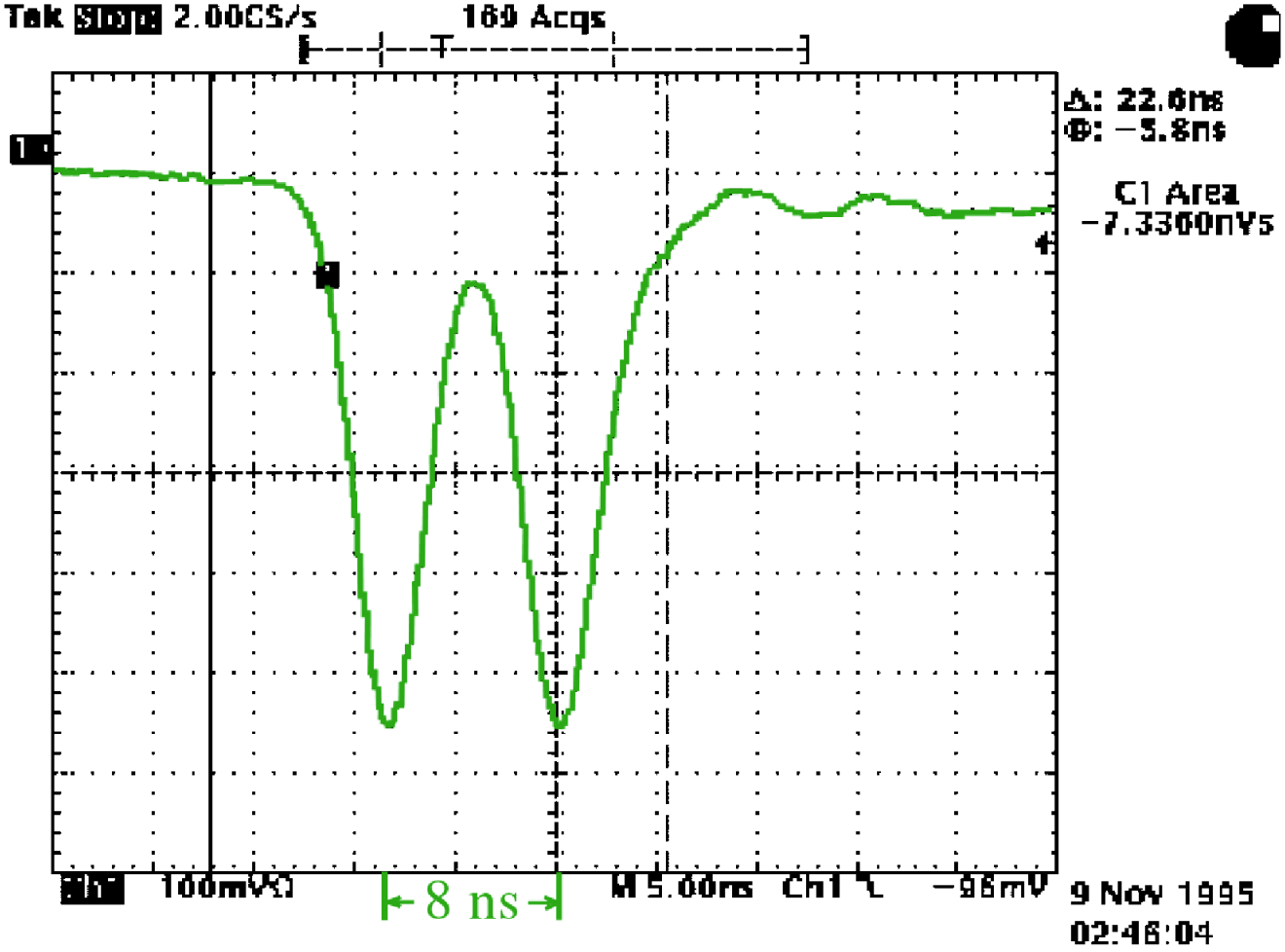

FIG. 7.19. Oscilloscope picture of two events separated by 8 ns in the Zero Degree Quartz Fiber Calorimeter of the NA50 experiment in the CERN heavy-ion beam [Arn 98].

e/π separation on the basis of time structure signals

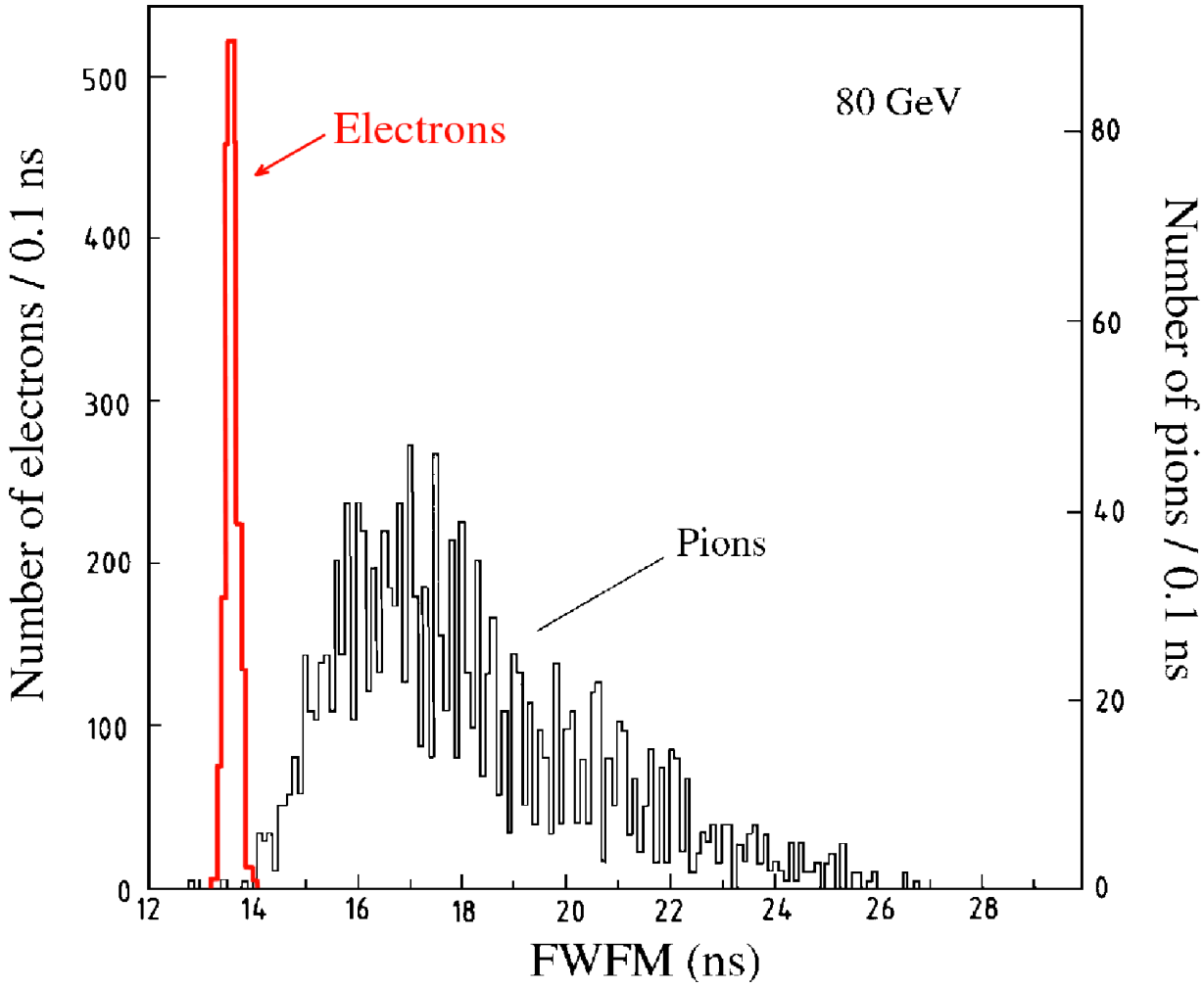

FIG. 7.33. The distribution of the full width at one-fifth maximum (FWFM) for 80 GeV electron and pion signals in SPACAL [Aco 91a]. The left-hand scale applies to the electron signals, the right-hand scale to the pion signals.

COURSE OUTLINE

- Calorimeters are *non-trivial* instruments,
  many *subtle effects conspire* to determine performance

Lecture themes:

1) ***The Physics of Shower Development***
2) ***The Calorimeter Response Function***
3) ***Practical Issues (Calibration, Operation, Simulation)***
4) ***Future Directions in Calorimetry (R&D)***

THE PHYSICS OF SHOWER DEVELOPMENT

Theme:

Even though calorimeters are intended to measure GeV, TeV energy deposits, their performance is determined by what happens at the MeV – keV – eV level

Electromagnetic showers

- *Electrons* lose energy by: *ionization* *radiation*

  Critical energy ϵ_c: $\frac{dE}{dx}$ (ion) $=$ $\frac{dE}{dx}$ (rad)

  $\epsilon_c \propto 1/Z$ PDG: $\epsilon_c = 610 \text{ MeV}/(Z + 1.24)$

- *Photons* interact by:

  1) *Photoelectric effect* $\sigma \propto Z^5,\ E^{-3}$

  2) *Compton scattering* $\sigma \propto Z,\ E^{-1}$

  3) *Conversion into* e^+e^- σ increases with E, Z, asymptotic at ~ 1 GeV

The *angular distribution* of photo- and Compton electrons is more or less *isotropic*, for the conversion electrons *directional*

Fundamentals of electromagnetic showers

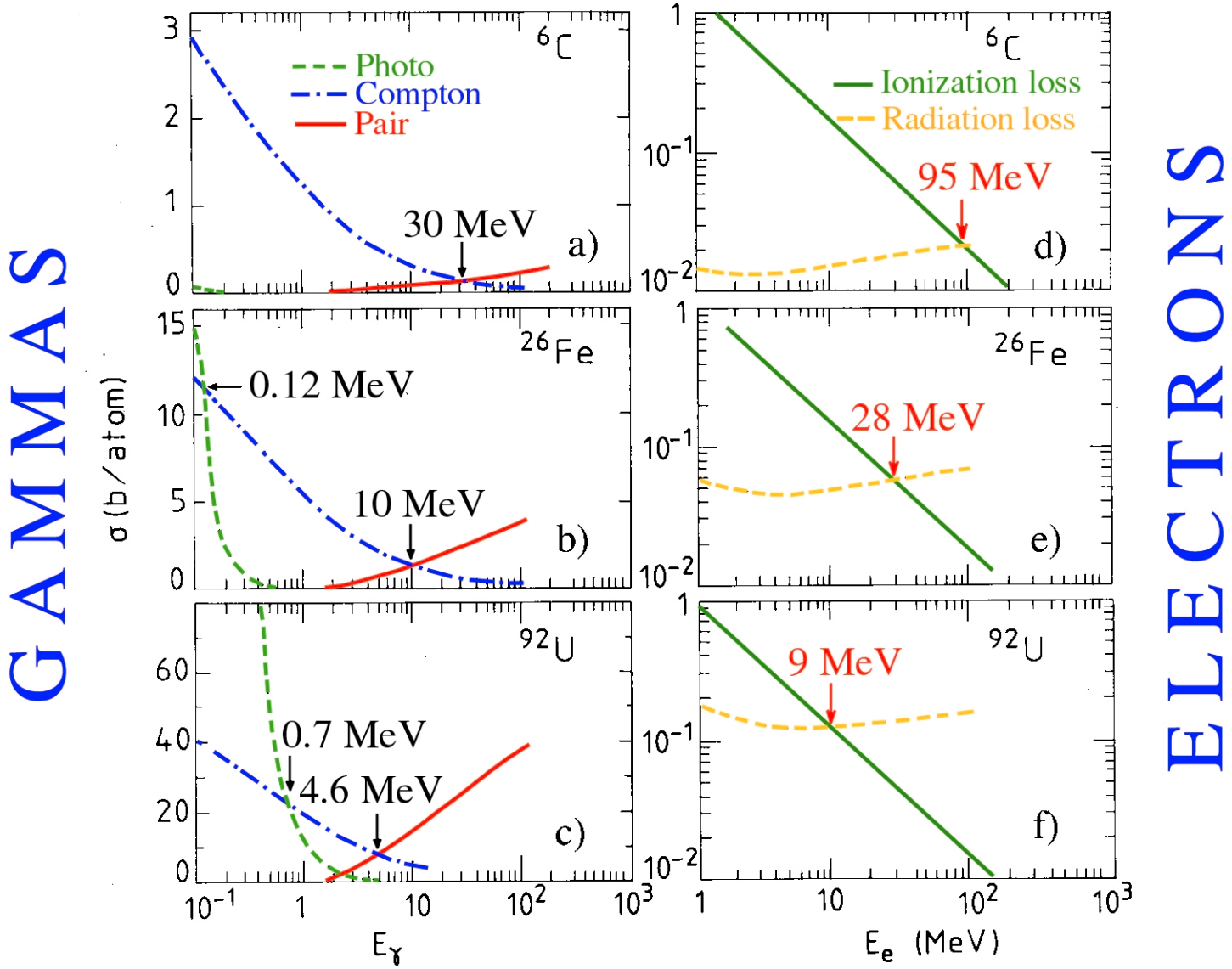

FIG. 2.1. Cross sections for the processes through which the particles composing electromagnetic showers lose their energy, in various absorber materials. To the left are shown the cross sections for pair production, Compton scattering and photoelectric effect in carbon (a), iron (b) and uranium (c). To the right, the fractional energy losses by radiation and ionization are given as a function of the electron energy in carbon (d), iron (e) and uranium (f).

Fundamentals of em showers: Critical energy

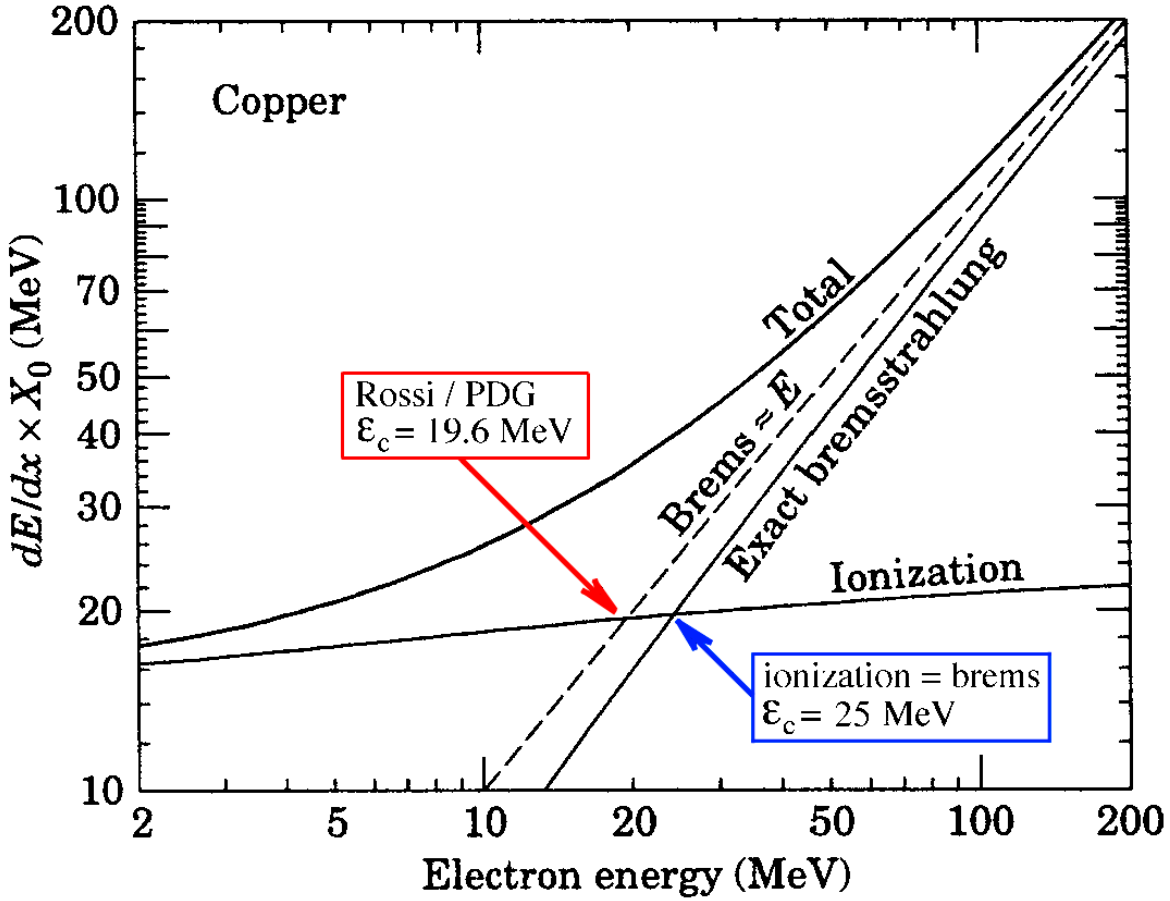

FIG. 2.2. Energy losses through ionization and bremsstrahlung by electrons in copper. The values for the critical energy following from the two definitions discussed in the text are indicated by arrows. From [PDG 98].

THE PHYSICS OF SHOWER DEVELOPMENT

Theme:

Even though calorimeters are intended to measure GeV, TeV energy deposits, their performance is determined by what happens at the MeV – keV – eV level

Electromagnetic showers

- *Electrons* lose energy by: *ionization* *radiation*

  Critical energy ϵ_c: $\frac{dE}{dx}$ (ion) $=$ $\frac{dE}{dx}$ (rad)

  $\epsilon_c \propto 1/Z$ PDG: $\epsilon_c = 610 \text{ MeV}/(Z + 1.24)$

- *Photons* interact by:

  1) *Photoelectric effect* $\sigma \propto Z^5,\ E^{-3}$

  2) *Compton scattering* $\sigma \propto Z,\ E^{-1}$

  3) *Conversion into* e^+e^- σ increases with E, Z, asymptotic at ~ 1 GeV

The *angular distribution* of photo- and Compton electrons is more or less *isotropic*, for the conversion electrons *directional*

Fundamentals of electromagnetic showers

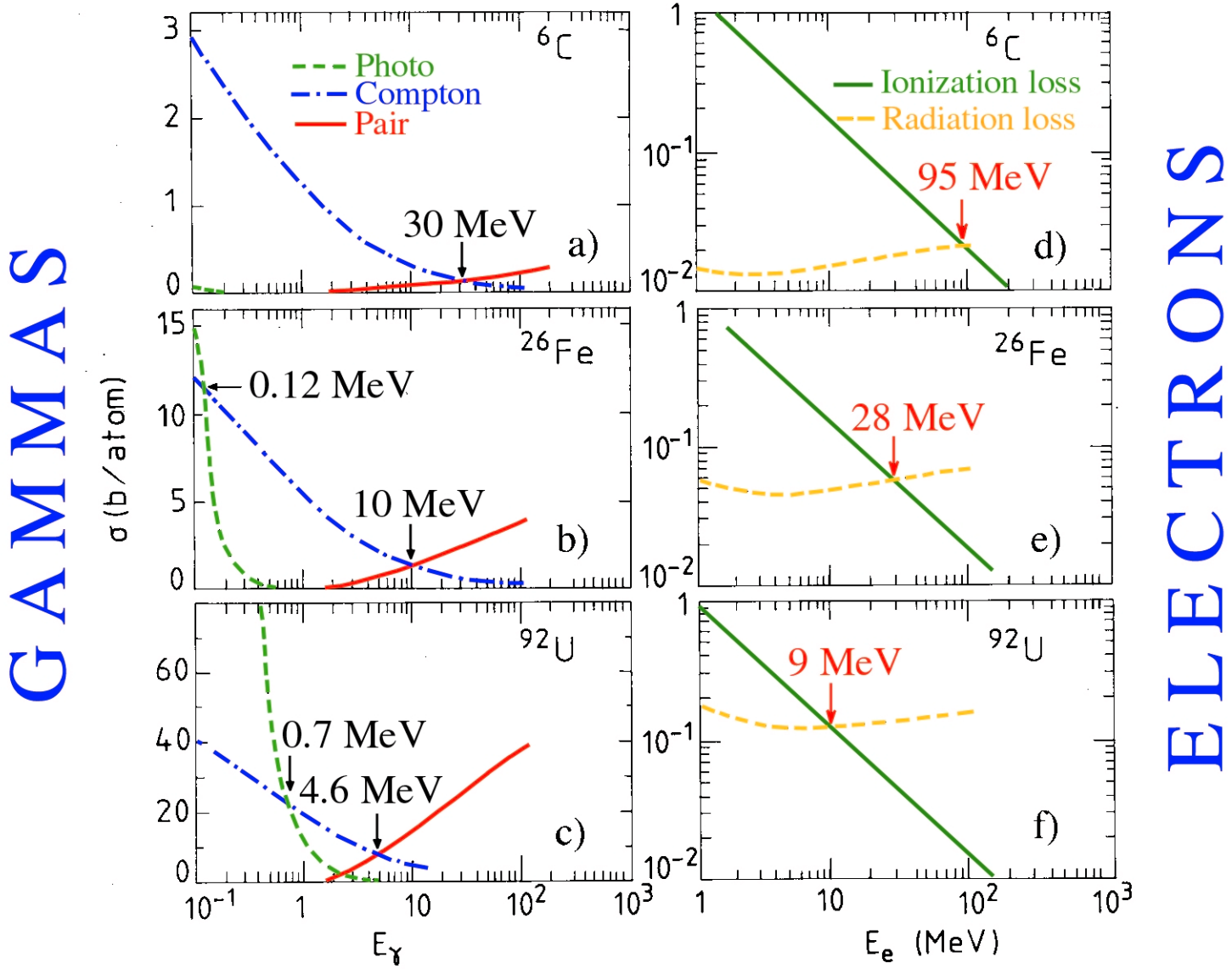

FIG. 2.1. Cross sections for the processes through which the particles composing electromagnetic showers lose their energy, in various absorber materials. To the left are shown the cross sections for pair production, Compton scattering and photoelectric effect in carbon (a), iron (b) and uranium (c). To the right, the fractional energy losses by radiation and ionization are given as a function of the electron energy in carbon (d), iron (e) and uranium (f).

Fundamentals of em showers: Photoelectric effect

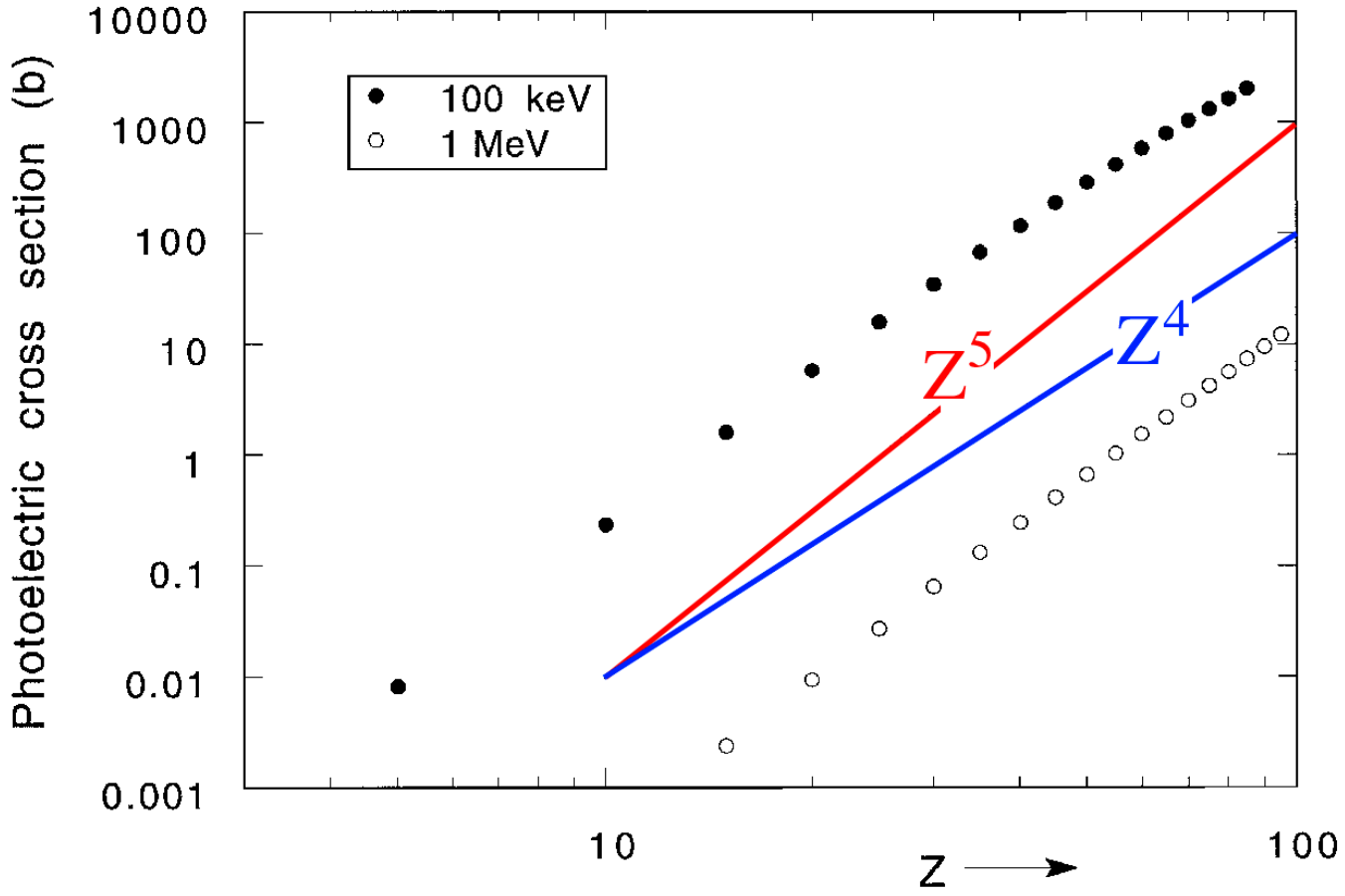

FIG. 2.3. Cross section for the photoelectric effect as a function of the Z value of the absorber. Data for 100 keV and 1 MeV γs.

Electromagnetic Showers

- Differences between high-Z/low-Z materials:
  - Energy at which *radiation* becomes dominant
  - Energy at which *photoelectric effect* becomes dominant
  - Energy at which e^+e^- *pair production* becomes dominant

- Showers $\rightarrow$ Particle *multiplication*
  100 GeV electrons: 90% of shower energy contained in 4 kg of lead

- Shower particle multiplicity reaches maximum at *shower maximum*
  Depth of shower maximum shifts logarithmically with energy

Fundamentals of em showers: Photon absorption

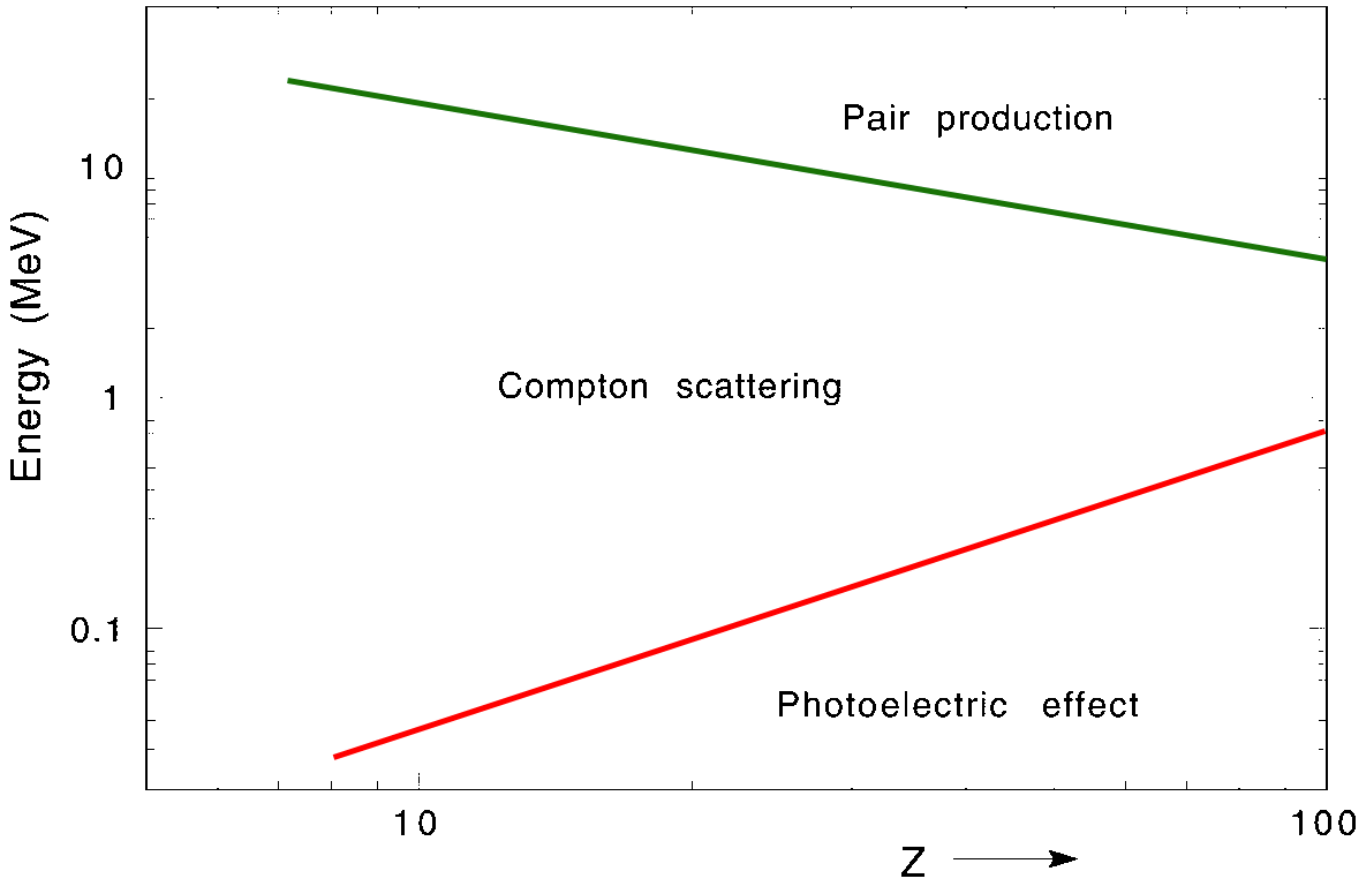

FIG. 2.7. The energy domains in which photoelectric effect, Compton scattering and pair production are the most likely processes to occur, as a function of the Z value of the absorber material.

Electromagnetic shower profiles (longitudinal)

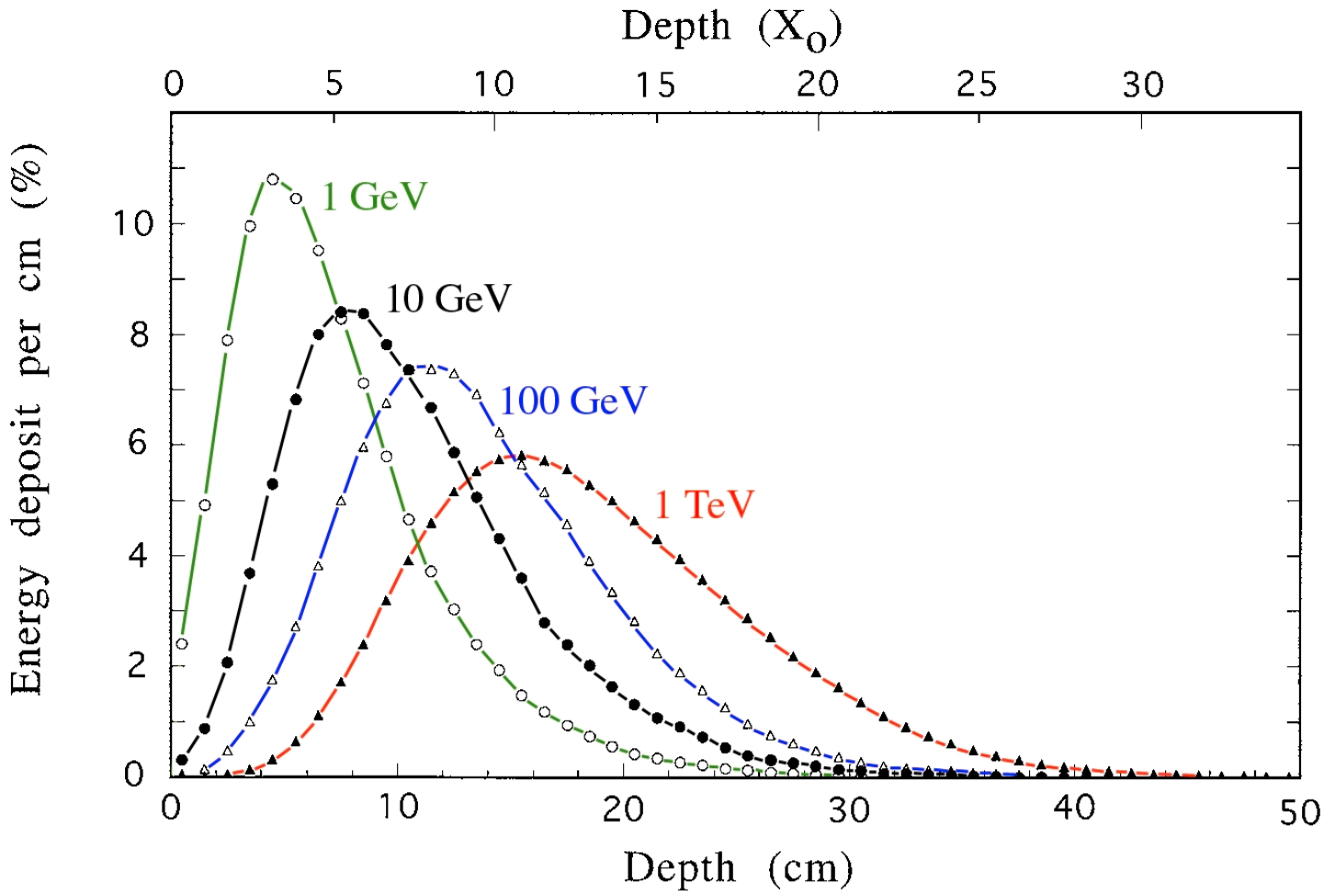

FIG. 2.9. The energy deposit as a function of depth, for 1, 10, 100 and 1000 GeV electron showers developing in a block of copper. In order to compare the energy deposit profiles, the integrals of these curves have been normalized to the same value. The vertical scale gives the energy deposit per cm of copper, as a percentage of the energy of the showering particle. Results of EGS4 calculations.

Electromagnetic Showers (2)

- *Longitudinal* development governed by *radiation length* (X_0)
  Defined for GeV regime:

$$X_0 = \frac{E}{(dE/dx)_{\rm rad}}$$

  Electron loses $\left[1 - 1/e\right] \approx 63\%$ of energy in 1 X_0
  The *mean free path* of a γ is 9/7 X_0 (asymptotic)

- There are important *differences between* showers induced by e, γ:
  e.g. Leakage fluctuations, effects of material upstream, ...

Electron / photon induced showers are different!

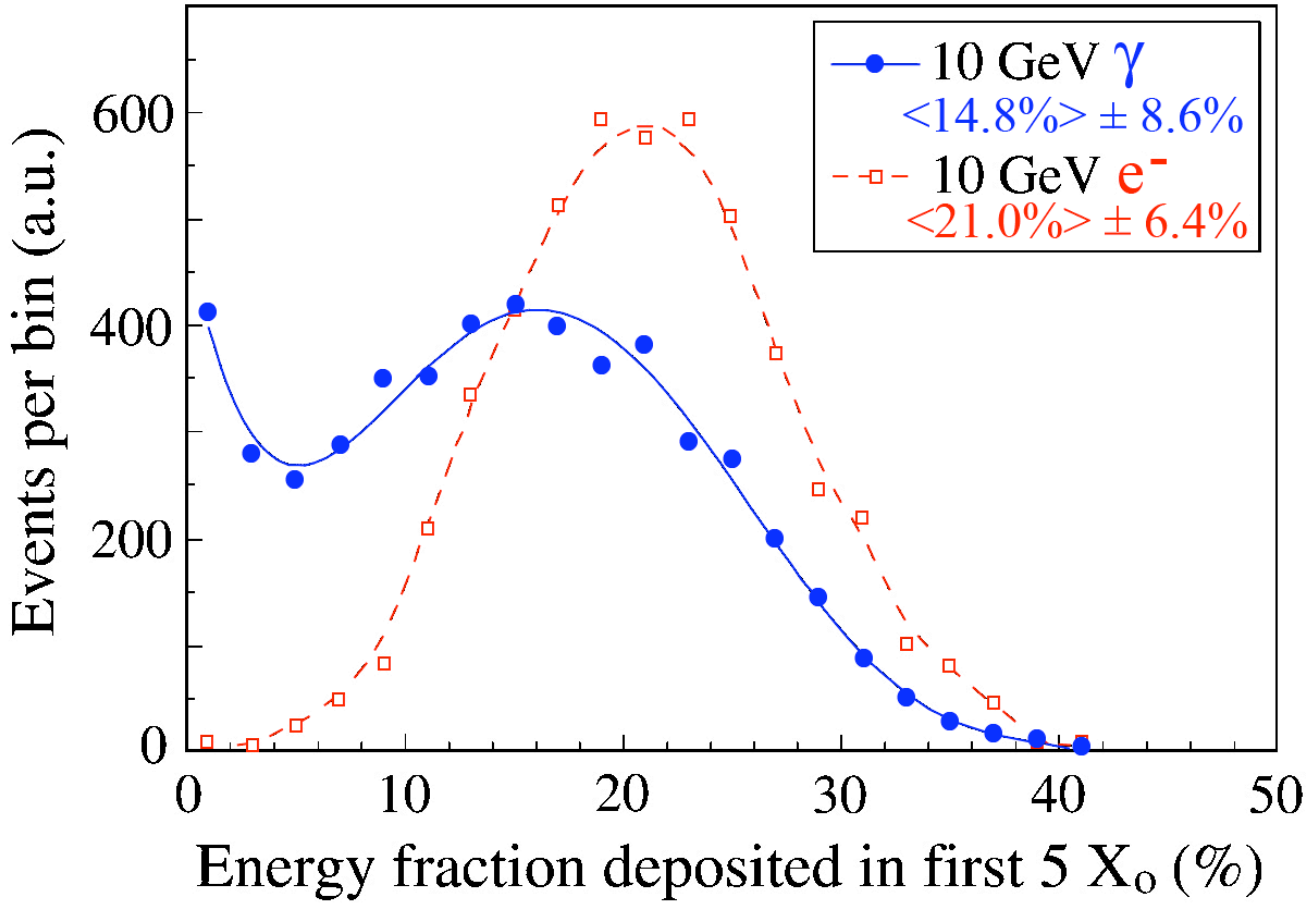

Figure 1: Distribution of the energy fraction deposited in the first 5 radiation lengths by 10 GeV electrons and γs showering in lead. Results of EGS4 simulations.

Electromagnetic Showers (3)

- *Scaling* with X_0 is *not perfect*
  In high-Z materials, particle multiplication continues longer and decreases more slowly than in low-Z materials
  Example: Number of e^+/GeV in Pb is 3 times larger than in Al
  ➡ *Need more* X_0 of *Pb* to contain showers at 99% level

Electromagnetic showers: Scaling is NOT perfect

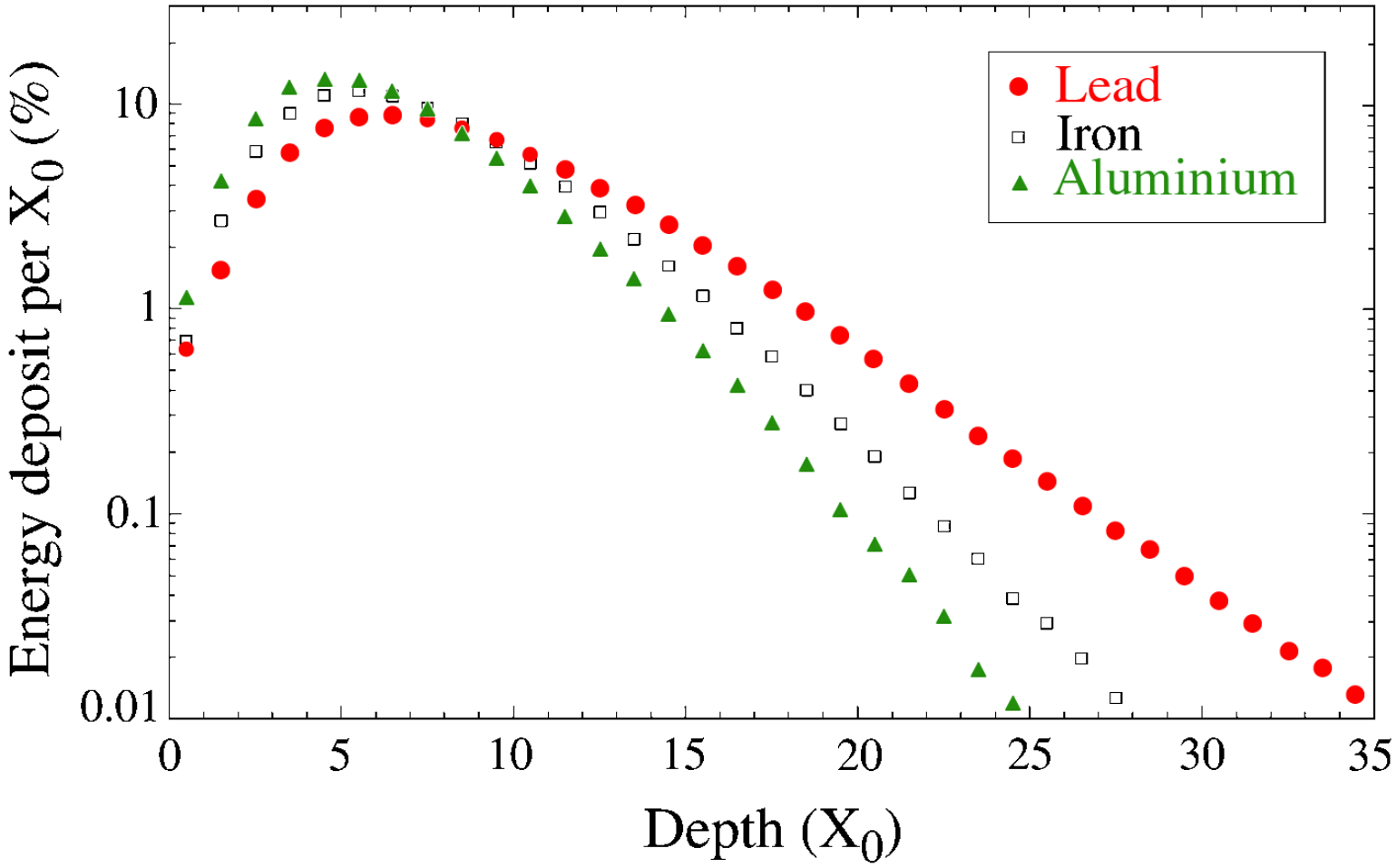

FIG. 2.12. Energy deposit as a function of depth, for 10 GeV electron showers developing in aluminium, iron and lead, showing approximate scaling of the longitudinal shower profile, when expressed in units of radiation length, X_0. Results of EGS4 calculations.

Electromagnetic shower leakage (longitudinal)

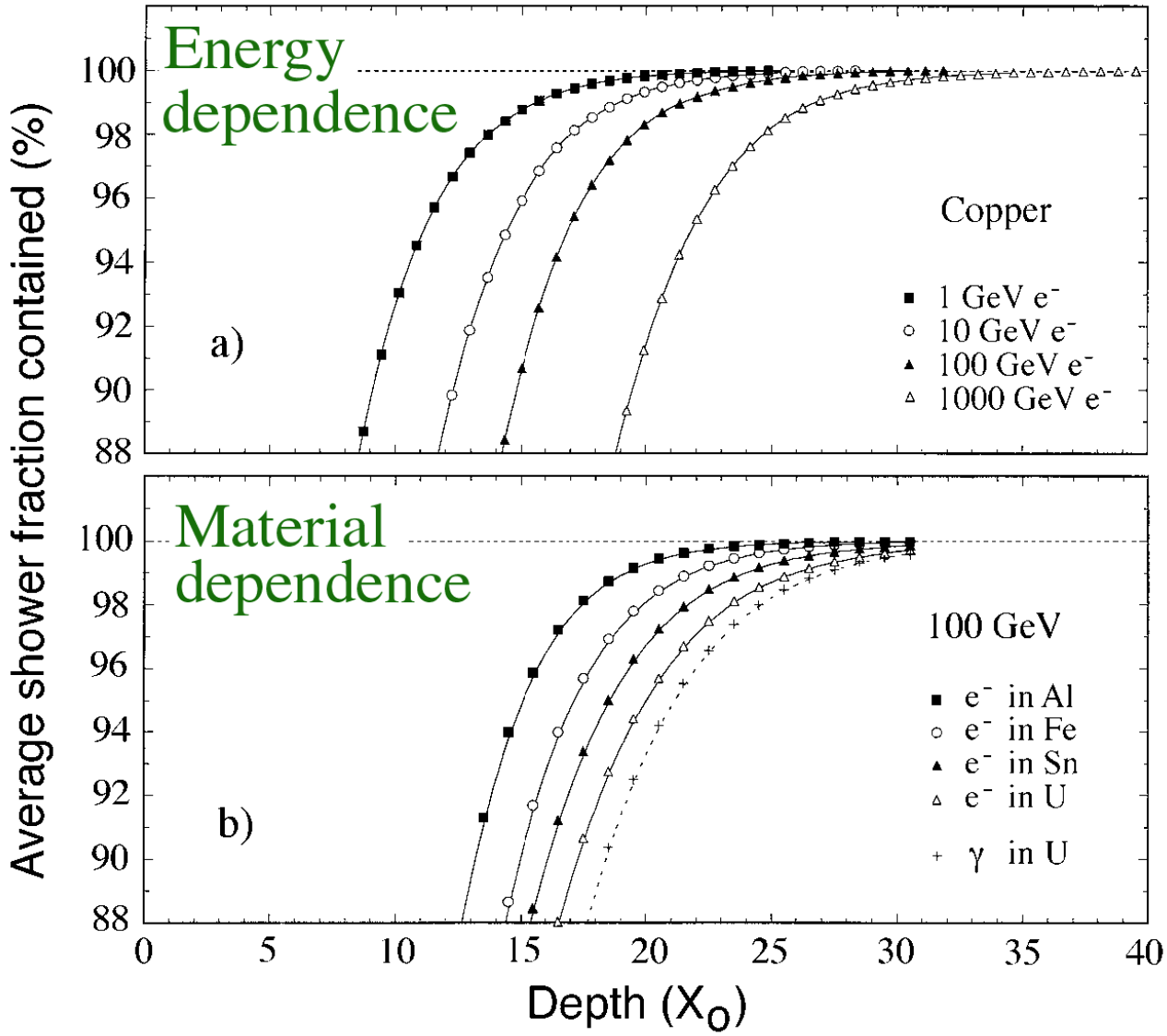

FIG. 2.17. Average energy fraction contained in a block of matter with infinite transverse dimensions, as a function of the thickness of this absorber. Shown are results for showers induced by electrons of various energies in a copper absorber (a) and results for 100 GeV electron showers in different absorber materials (b). The lower figure also shows the results for 100 GeV γ showers in ^{238}U. Results of EGS4 calculations.

Electromagnetic Showers (4)

- Phenomena at $E < \varepsilon_c$ determine important calorimeter properties
  In lead, $> 40\%$ of energy deposited by $e^{\pm}$ with $E < 1$ MeV
  Only 1/4 deposited by e^+, 3/4 by e^- (Compton, photo electrons!)
  The e^+ are closer to the shower axis, Compton & p.e. in halo

Electromagnetic showers: The importance of SOFT shower particles

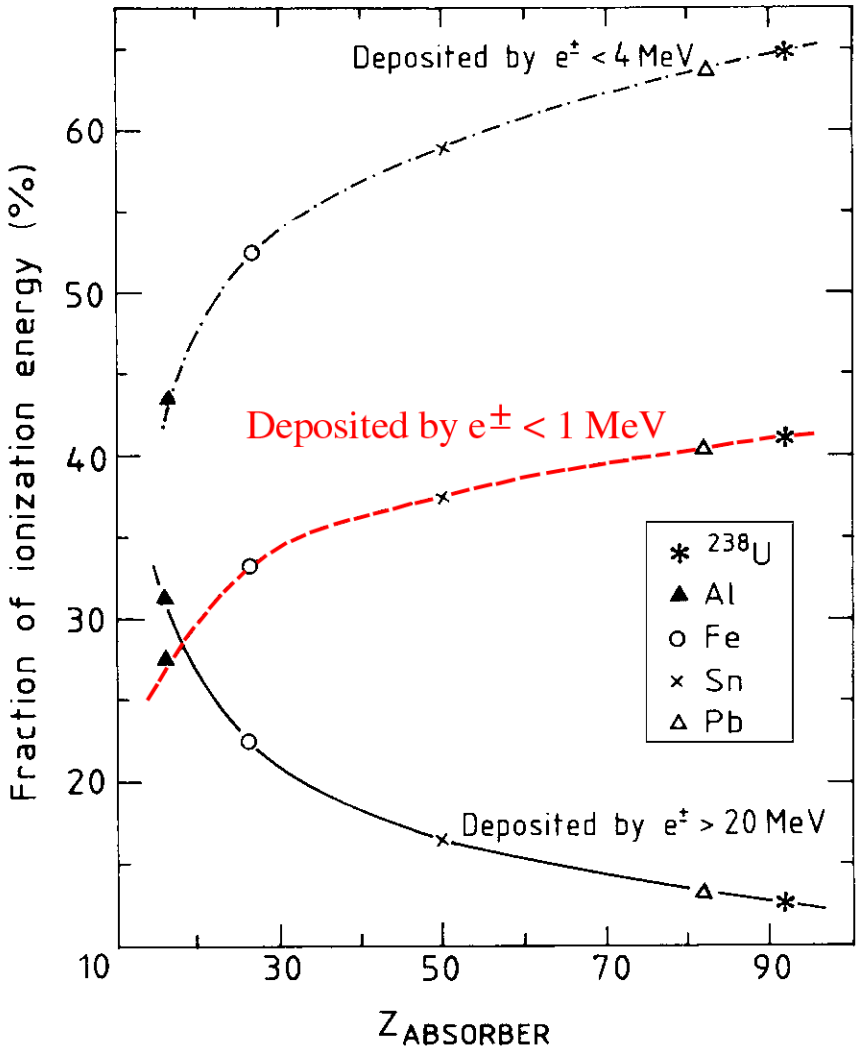

FIG. 2.10. The composition of em showers. Shown are the percentages of the energy of 10 GeV electromagnetic showers deposited through shower particles with energies below 1 MeV (the dashed curve), below 4 MeV (the dash-dotted curved) or above 20 MeV (the solid curve), as a function of the Z of the absorber material. Results of EGS4 simulations.

Electromagnetic showers: Contributions e^+,e^- to signals

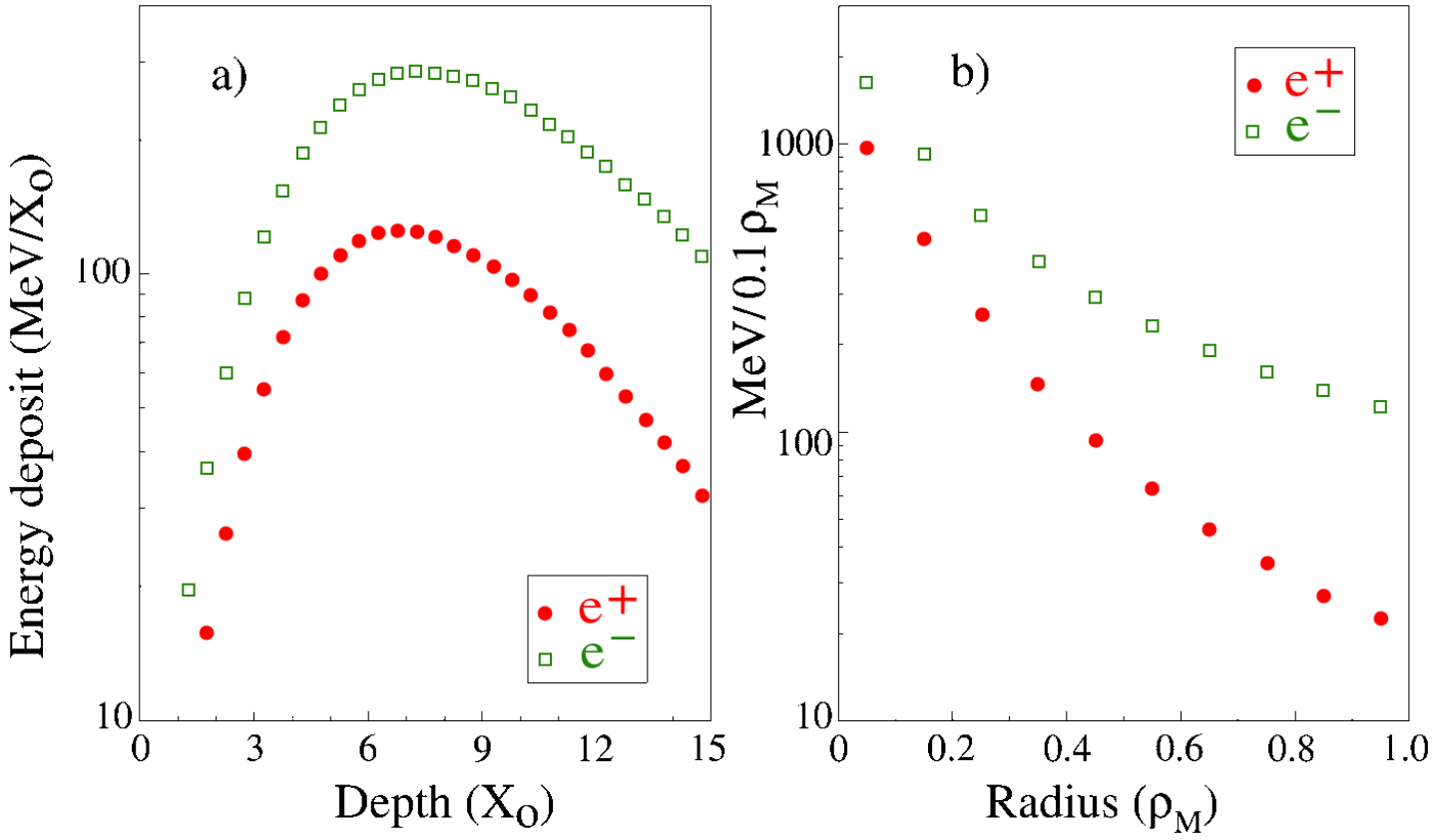

FIG. 2.11. Comparison of the longitudinal (a) and lateral (b) profiles of the energy deposited by electrons and positrons in 10 GeV em showers developing in lead. Note the logarithmic vertical scale. Results from EGS4 simulations.

Electromagnetic Showers (5)

- *Lateral* shower width determined by
  - *Multiple scattering* of e^+, e^- (early, 0.2 ρ_M)
  - *Compton* γ*s* travelling away from axis (1 - 1.5 ρ_M)

  Scaling with Molière radius $\rho_M \propto X_0/\epsilon_c$
  $X_0 \propto A/Z^2,\ \epsilon_c \propto 1/Z\ \rightarrow \rho_M \propto A/Z$

Electromagnetic showers: Lateral profile, depth dependence

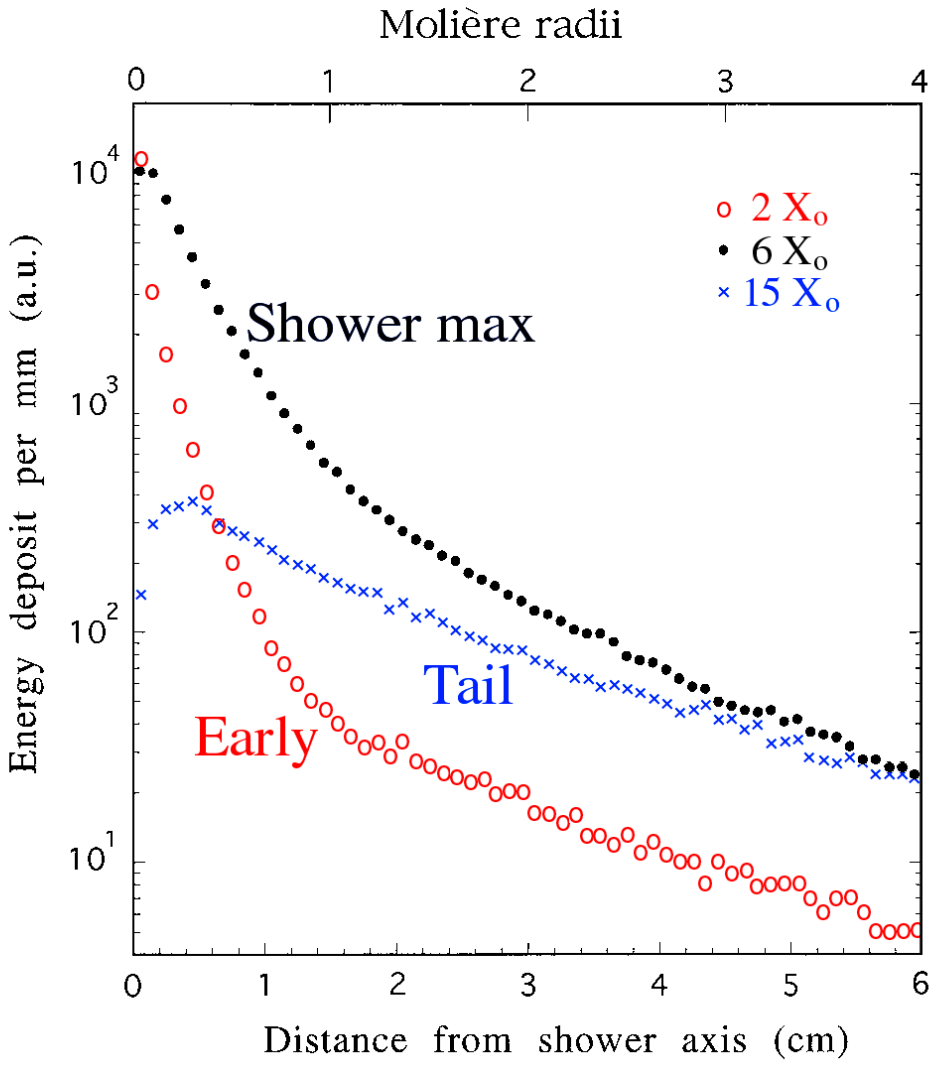

FIG. 2.13. The radial distributions of the energy deposited by 10 GeV electron showers in copper, at various depths. Results of EGS4 calculations.

Em showers: Lateral profiles, material dependence

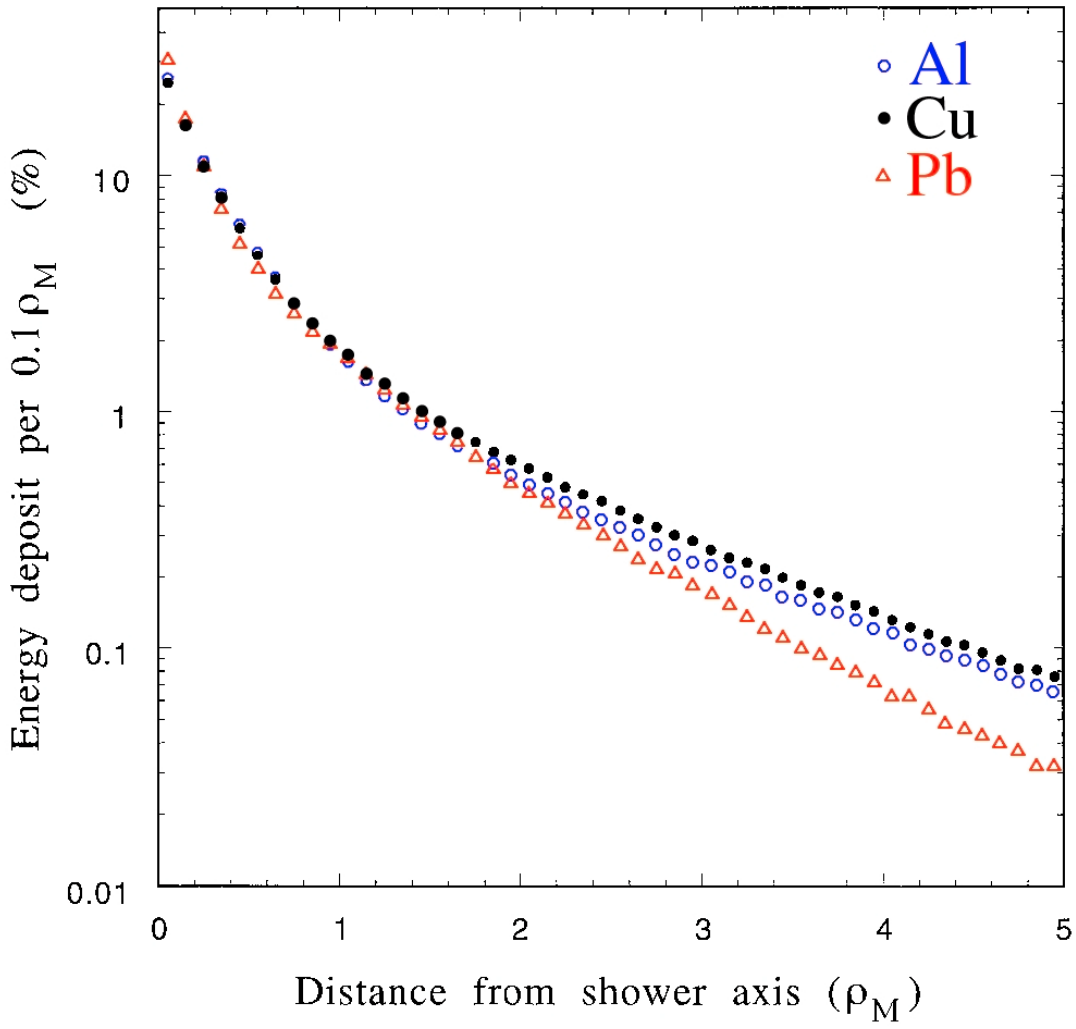

FIG. 2.14. Radial energy deposit profiles for 10 GeV electrons showering in aluminium, iron and lead. Results of EGS4 calculations.

Electromagnetic shower leakage (lateral)

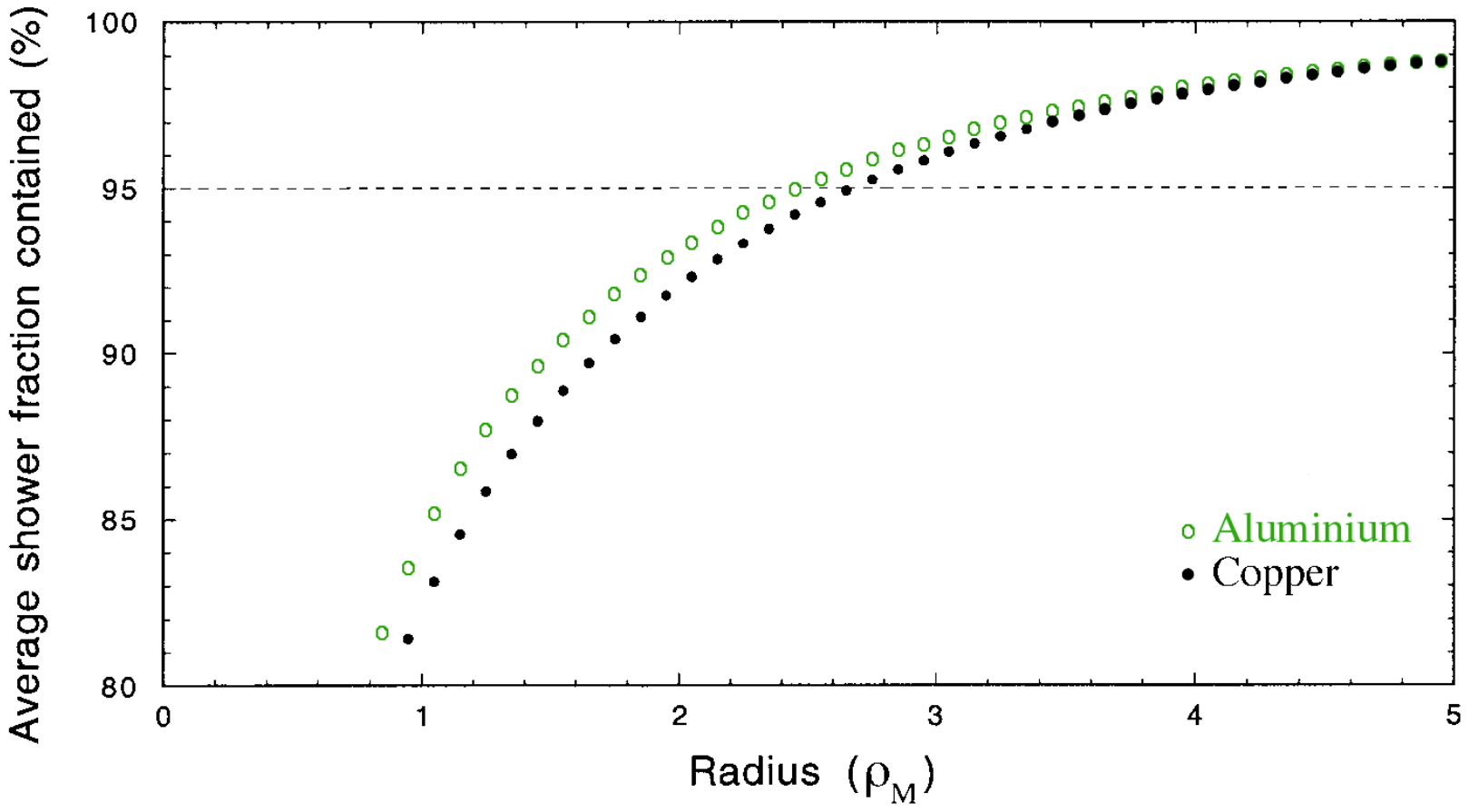

FIG. 2.18. Average energy fraction contained in an infinitely long cylinder of absorber material, as a function of the radius of this cylinder. Results of EGS4 calculations for various absorber materials and different energies.

Electromagnetic shower profiles: Experimental data

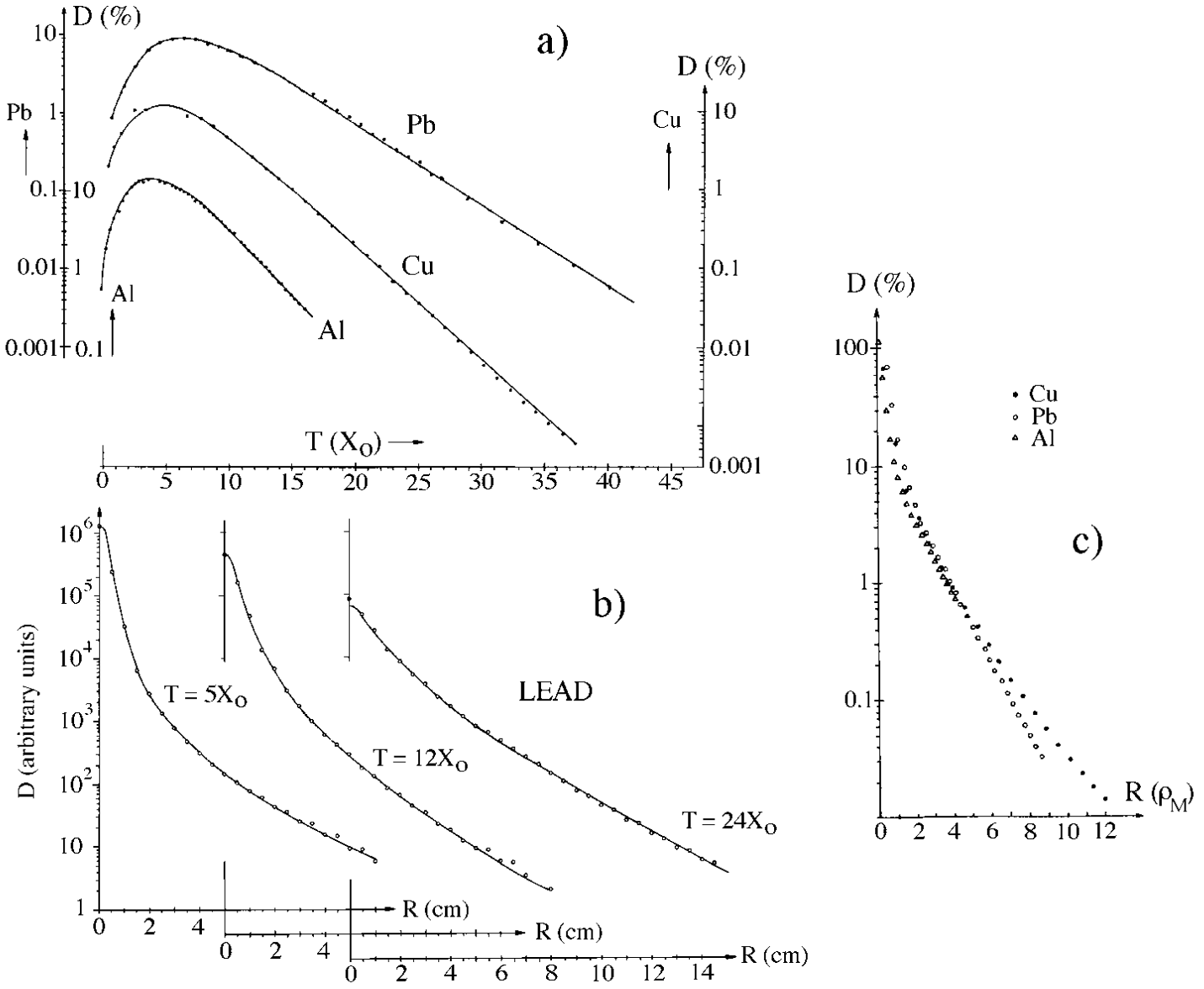

FIG. 2.16. Experimental results on the shower profiles of 6 GeV electrons in aluminium, copper and lead. Shown are the longitudinal profiles in these three materials (a), the lateral profiles in lead, measured at 3 different depths (b), and the integrated lateral profiles for copper and lead (c). Data from [Bat 70].

Intermezzo: On Čerenkov fiber calorimeters

- *Čerenkov* light is emitted by *relativistic charged* particles ($\beta > 1/n$)
  e.g. quartz ($n = 1.45$): Threshold 0.2 MeV for e, 400 MeV for p

  Light is emitted at angle $\theta = \arccos(\beta n)^{-1}$ ($\sim 45^\circ$ for $\beta \sim 1$ in quartz)

- *Optical fibers* only trap light emitted within the *numerical aperture*

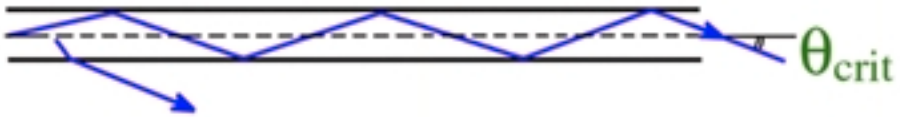

$\theta_{crit} \sim 20^\circ$ for quartz fibers

- Comparison of *Čerenkov* light (directional) and *scintillation* light (isotropic) produced in fiber calorimeters is a rich source of information on details of shower development

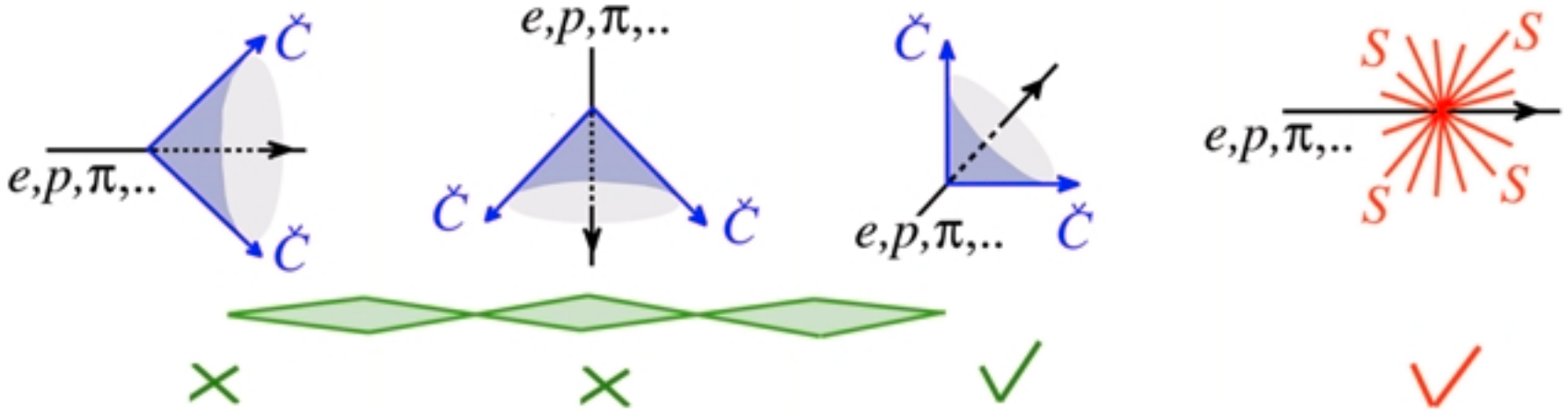

DREAM: A calorimeter with Čerenkov and scintillating fibers

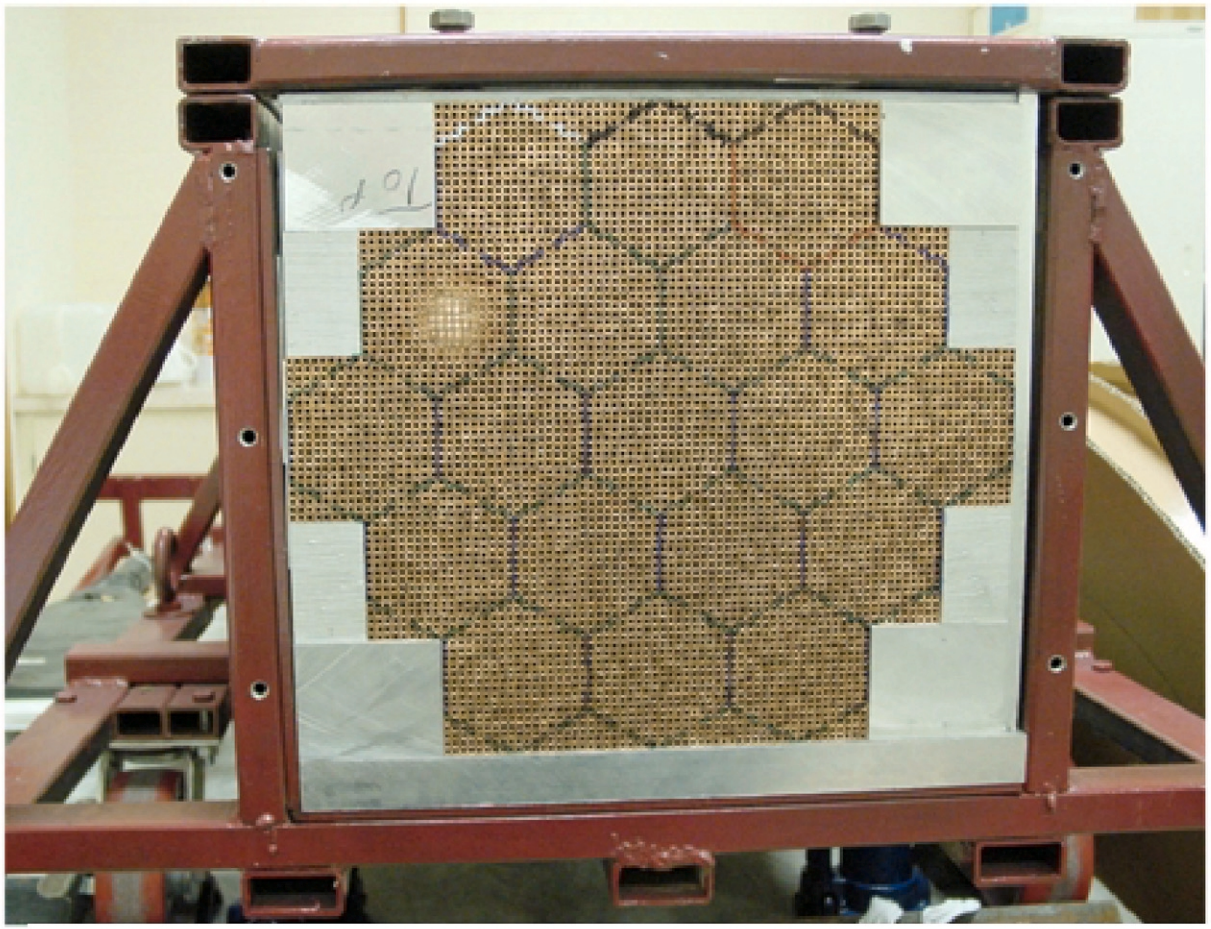

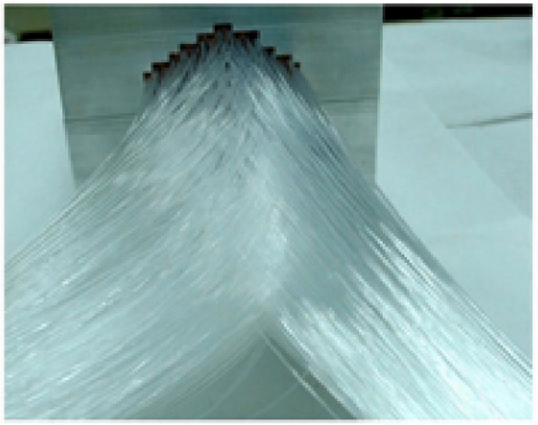

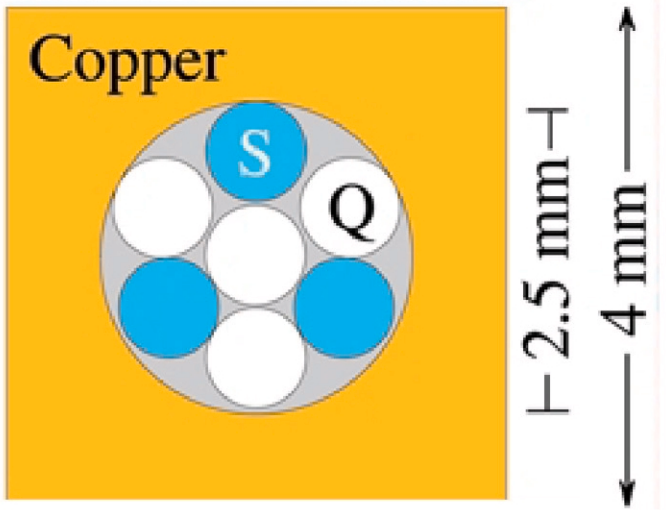

The changing angular distribution of shower particles

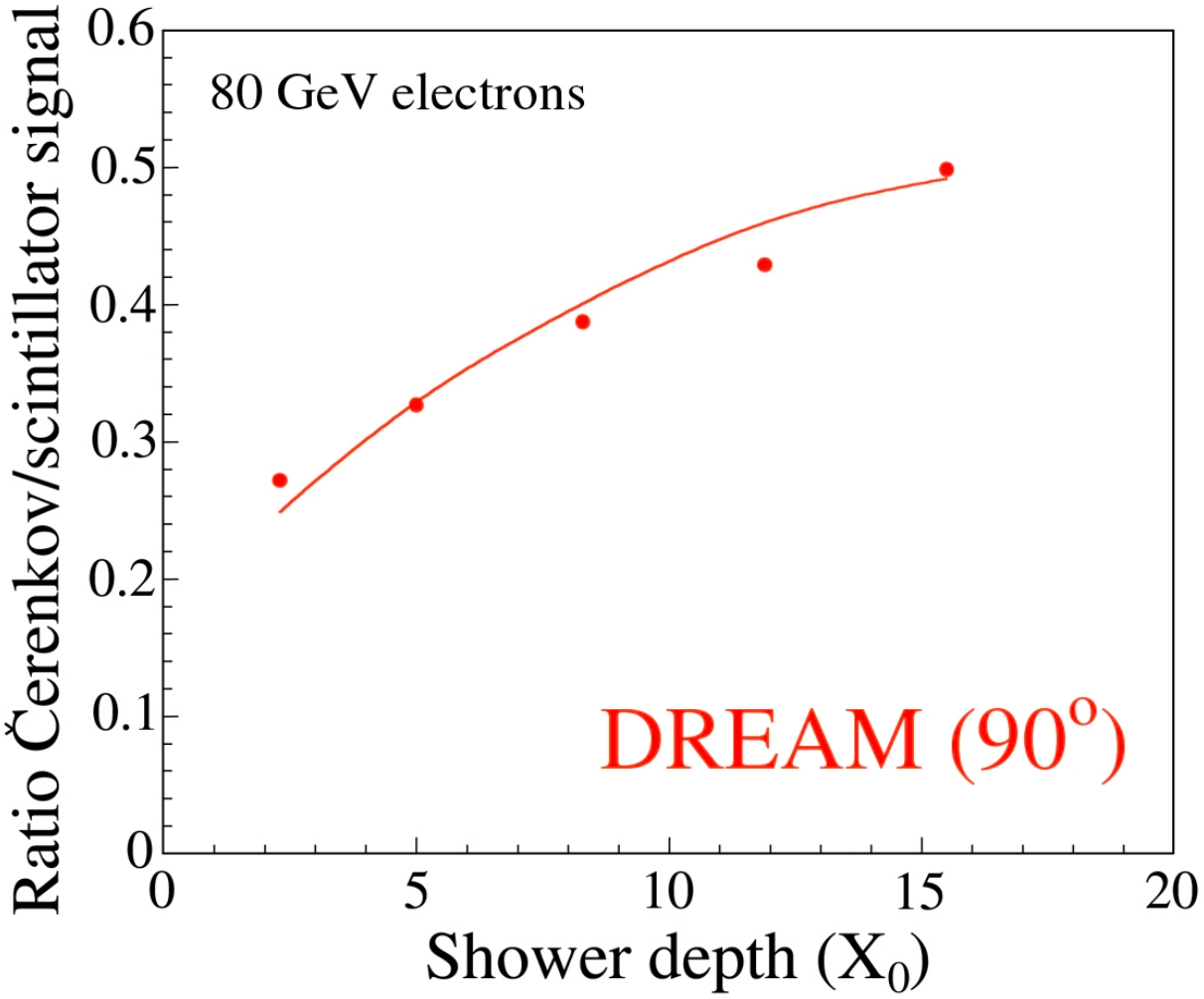

Electromagnetic showers: Lateral profile, depth dependence

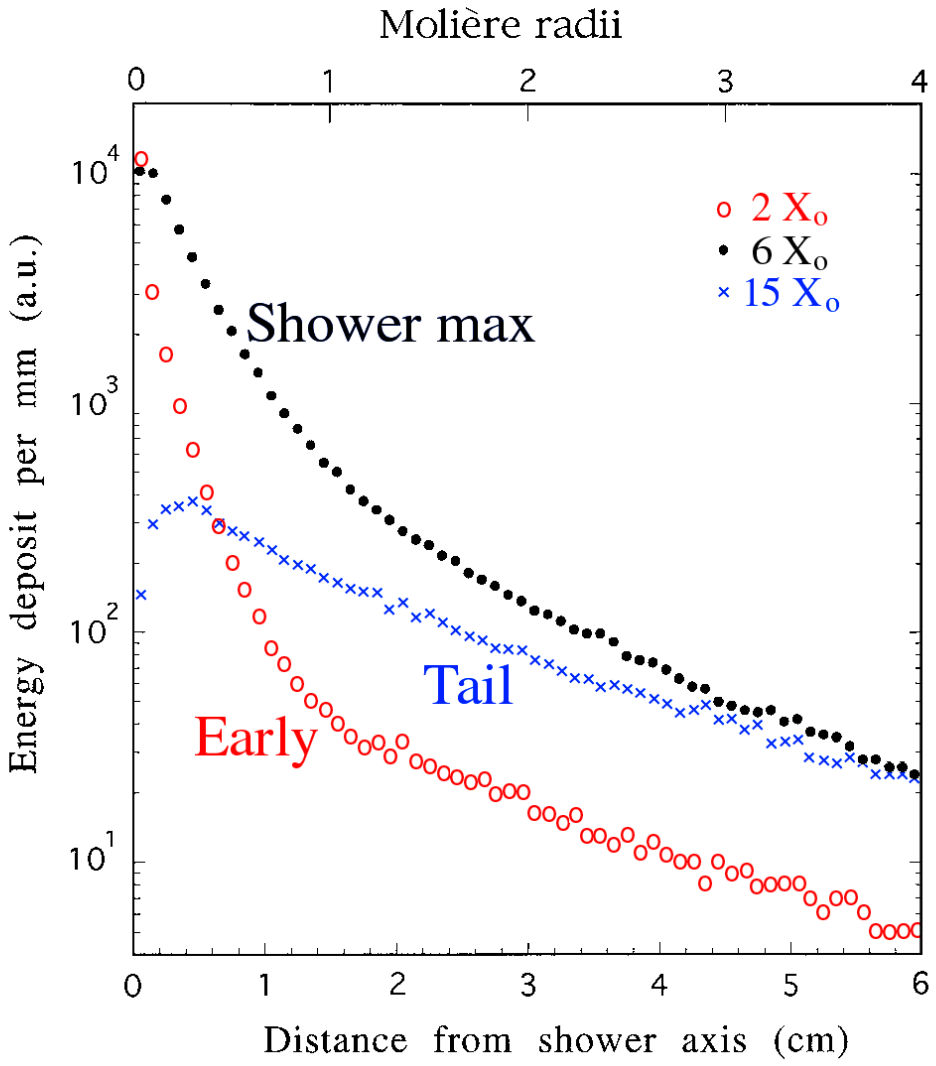

FIG. 2.13. The radial distributions of the energy deposited by 10 GeV electron showers in copper, at various depths. Results of EGS4 calculations.

Muons in calorimeters

- *Muons are not minimum ionizing particles (mip's)*

$$\epsilon_c(\mu) = \left[\frac{m_\mu}{m_e}\right]^2 \times \epsilon_c(e)$$

$\rightarrow \epsilon_c(\mu) \approx 200$ GeV in Pb.

The effects of radiation are clearly visible in calorimeters, especially for high-energy muons in high-Z absorber material

Muon signals in a calorimeter

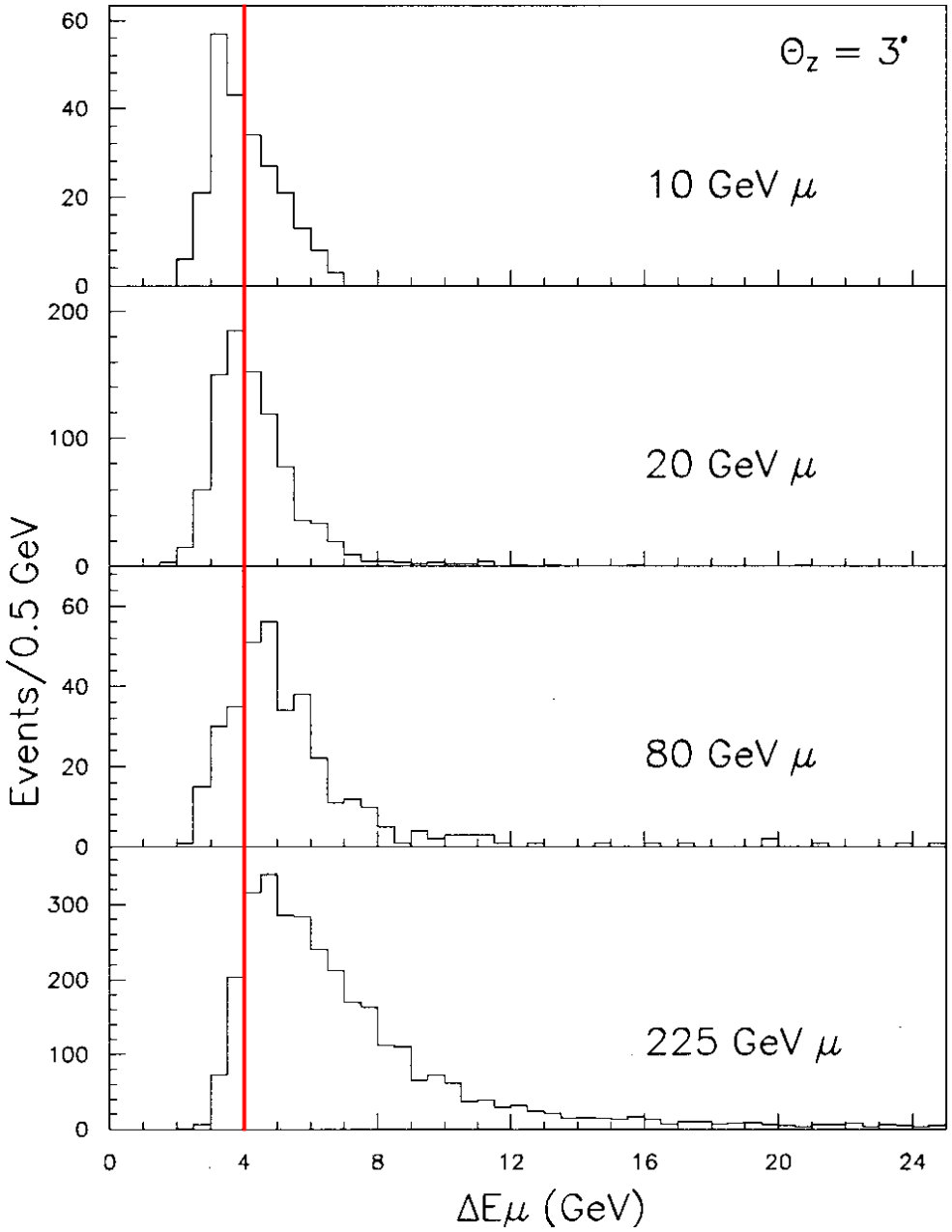

FIG. 2.19. Signal distributions for muons of 10, 20, 80 and 225 GeV traversing the $9.5\lambda_{\rm int}$ deep SPACAL detector at $\theta_z = 3^\circ$. From [Aco 92c].

Calorimetric separation of ionization / radiation losses

Muon signals in the DREAM calorimeter

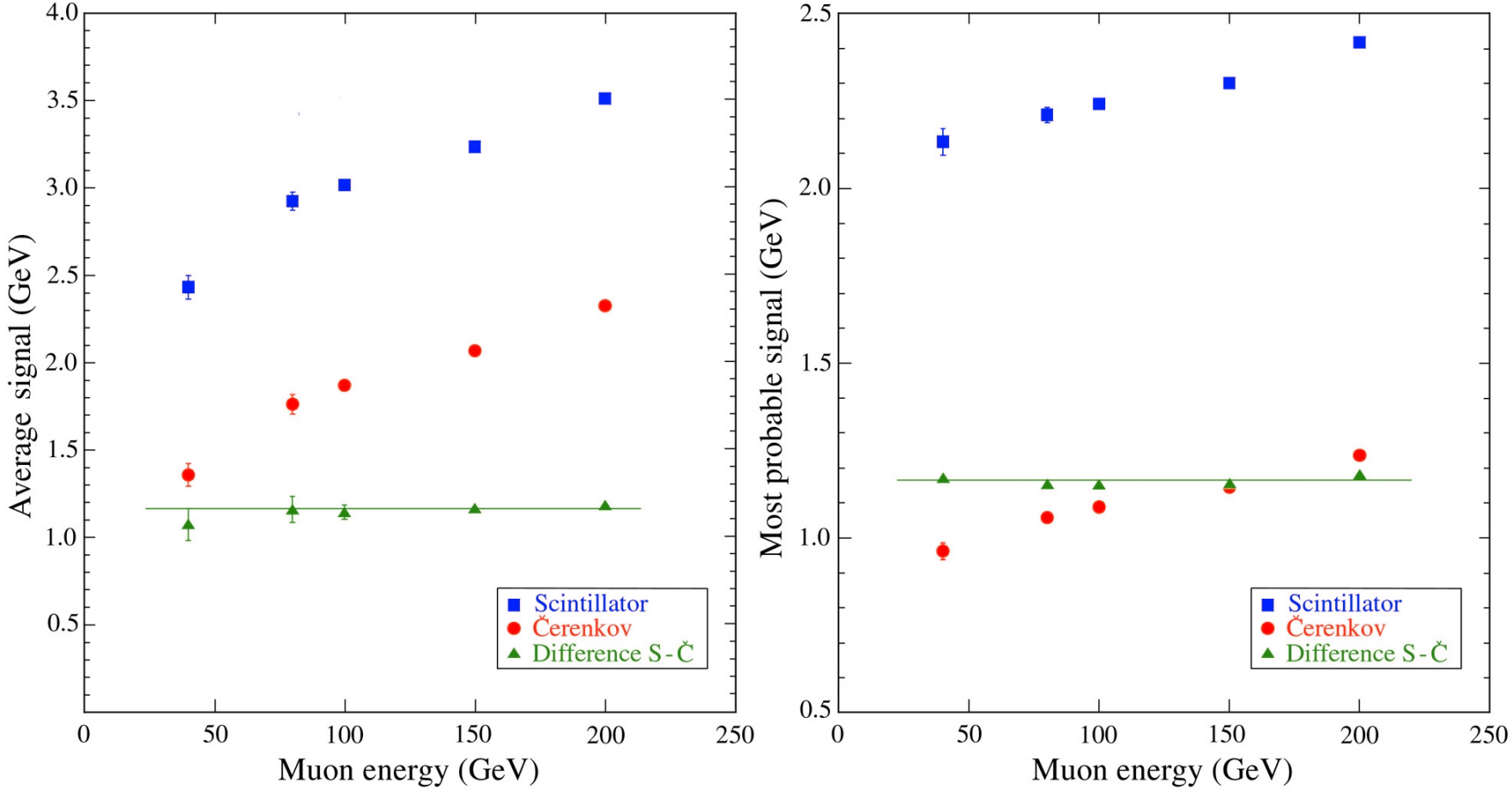

from: NIM A533 (2004) 305

Hadron Showers (1)

- Extra complication: ***The strong interaction***

  - Production of other particles, mainly pions
    Some of these particles (π^0, η) develop *electromagnetic showers*
  - *Nuclear reactions*: protons, neutrons released from nuclei
    ➡ *Invisible energy* (nuclear binding energy, target recoil)

Hadron shower fundamentals: A typical process

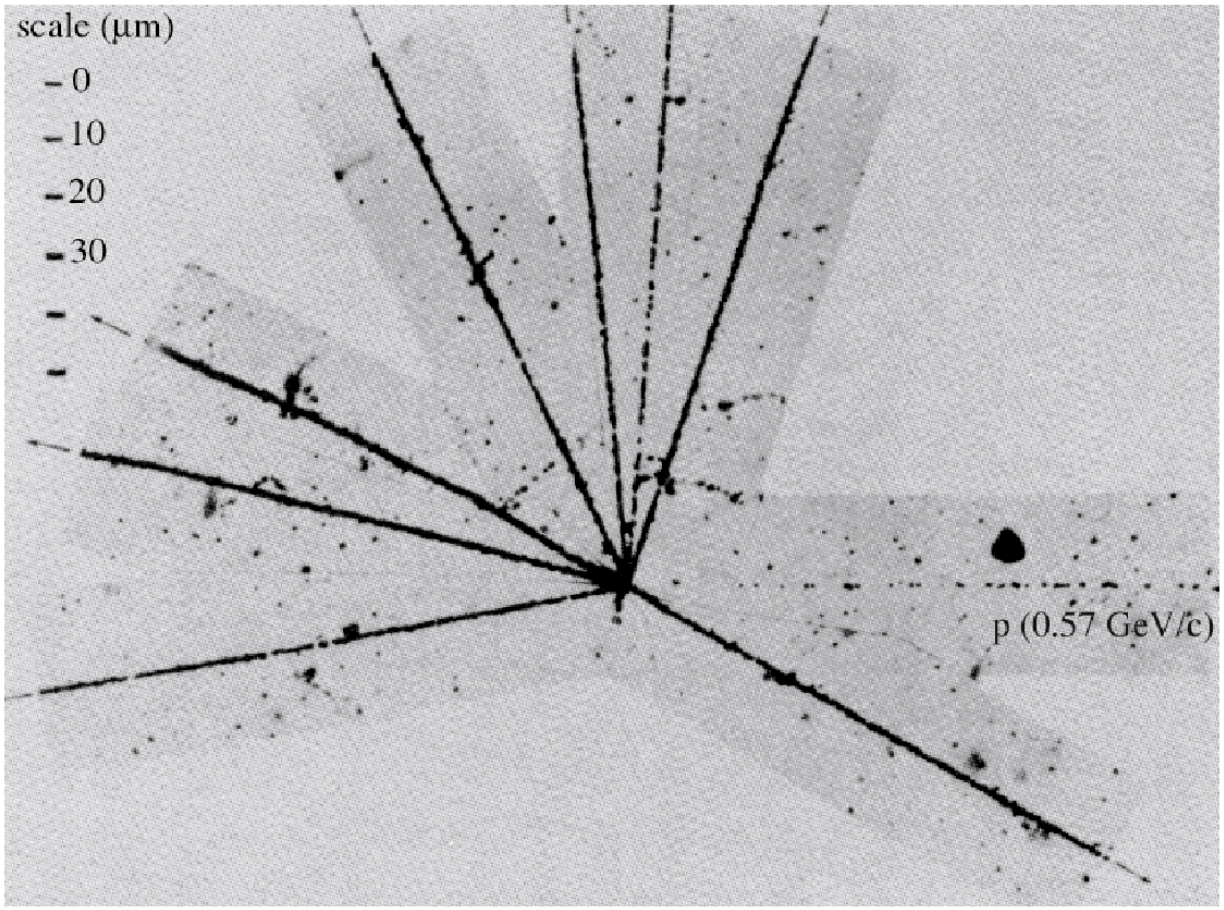

FIG. 2.42. A nuclear interaction induced by a proton with a kinetic energy of 160 MeV in a nuclear emulsion stack. Photograph courtesy CERN.

Hadron Showers (2)

- Breakdown of ***non-em*** energy deposit in lead absorber:
  - *Ionizing particles* *56%* (2/3 from spallation protons)
  - *Neutrons* *10%* (37 neutrons per GeV!)
  - *Invisible* *34%*

Spallation protons carry typically 100 MeV,
Evaporation neutrons 3 MeV

Hadron shower fundamentals: Where does the energy go?

	Lead	*Iron*
Ionization by pions	19%	21%
Ionization by protons	37%	53%
Total ionization	56%	74%
Nuclear binding energy loss	32%	16%
Target recoil	2%	5%
Total invisible energy	34%	21%
Kinetic energy evaporation neutrons	10%	5%
Number of charged pions	0.77	1.4
Number of protons	3.5	8
Number of cascade neutrons	5.4	5
Number of evaporation neutrons	31.5	5
Total number of neutrons	36.9	10
Neutrons/protons	10.5/1	1.3/1

Table 2.5 *Energy deposit and composition of the non-em component of hadronic showers in lead and iron. The listed numbers of particles are per GeV of non-em energy*

Hadron shower fundamentals: Neutron production spectra

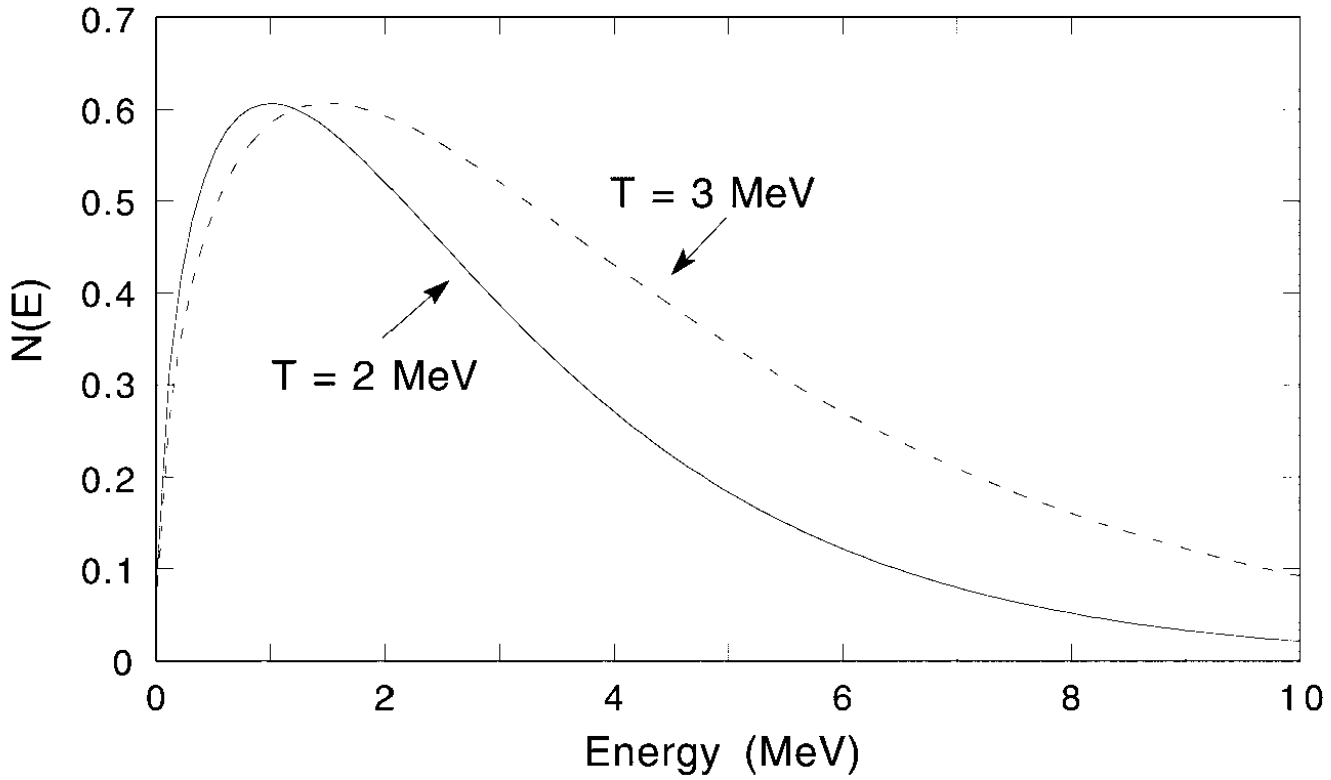

FIG. 2.29. Kinetic energy spectrum of evaporation neutrons, produced according to a Maxwell distribution with a temperature of 2 MeV. For comparison, the spectrum for a temperature of 3 MeV is given as well.

Hadron showers (4)
The electromagnetic fraction, f_{em}

- The (average) em shower fraction is *energy dependent*
  (π^0 production is a one-way street)

$$\langle f_{\mathrm{em}} \rangle \;=\; 1 \;-\; \left[\frac{2}{3}\right]^{n} \;=\; 1 \;-\; \left[\frac{E}{E_0}\right]^{k-1}$$

  with n the number of generations, $k-1$ the multiplicity and E_0 the average energy needed for the production of a π
  $\longrightarrow \langle f_{\mathrm{em}} \rangle$ is also somewhat *Z dependent*

- ***Consequences:***
  - Signal of pion $<$ signal of electron *(non-compensation)*
  - e/π signal ratio energy dependent *(non-linearity)*

Hadron showers: Energy dependence em component

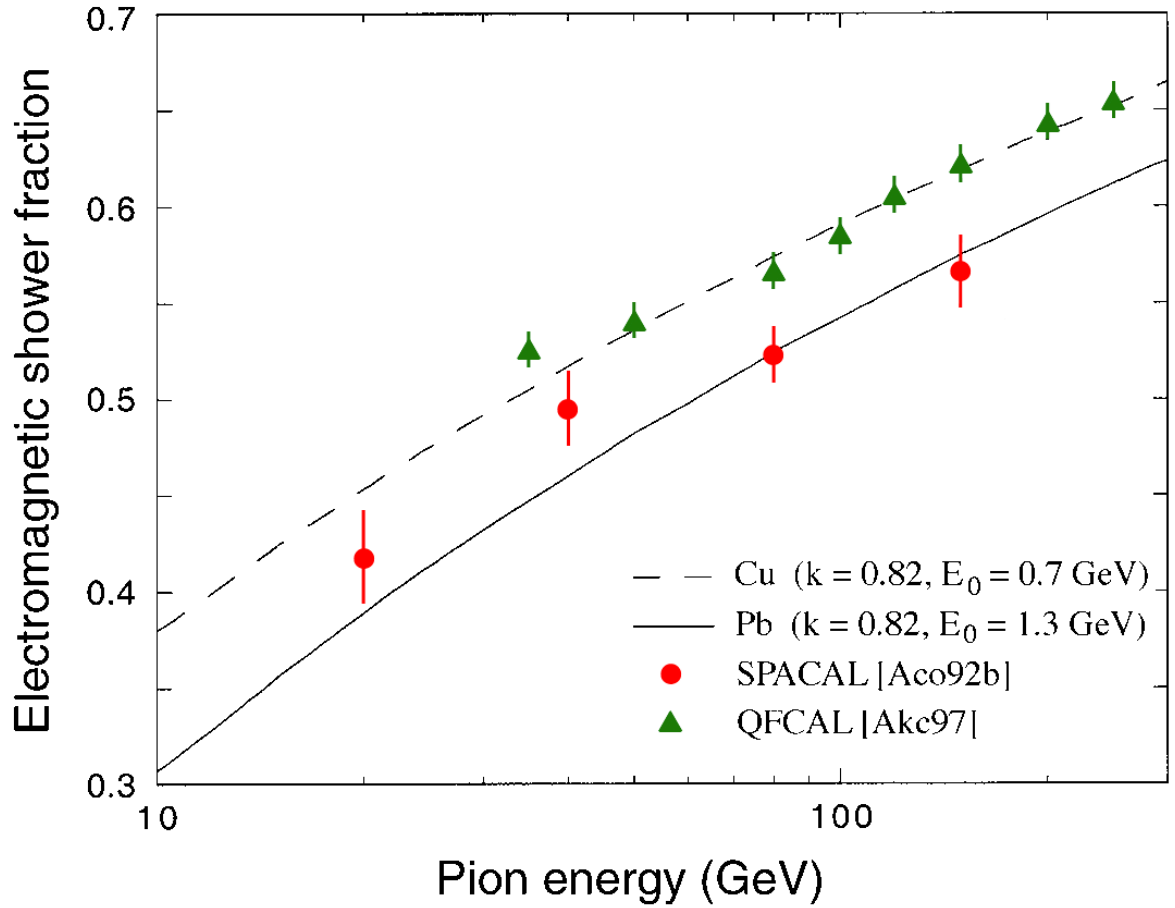

FIG. 2.22. Comparison between the experimental results on the em fraction of pion-induced showers in the (copper-based) QFCAL and (lead-based) SPACAL detectors. Data from [Akc 97] and [Aco 92b].

Hadronic signal (non-)linearity: Dependence on e/h

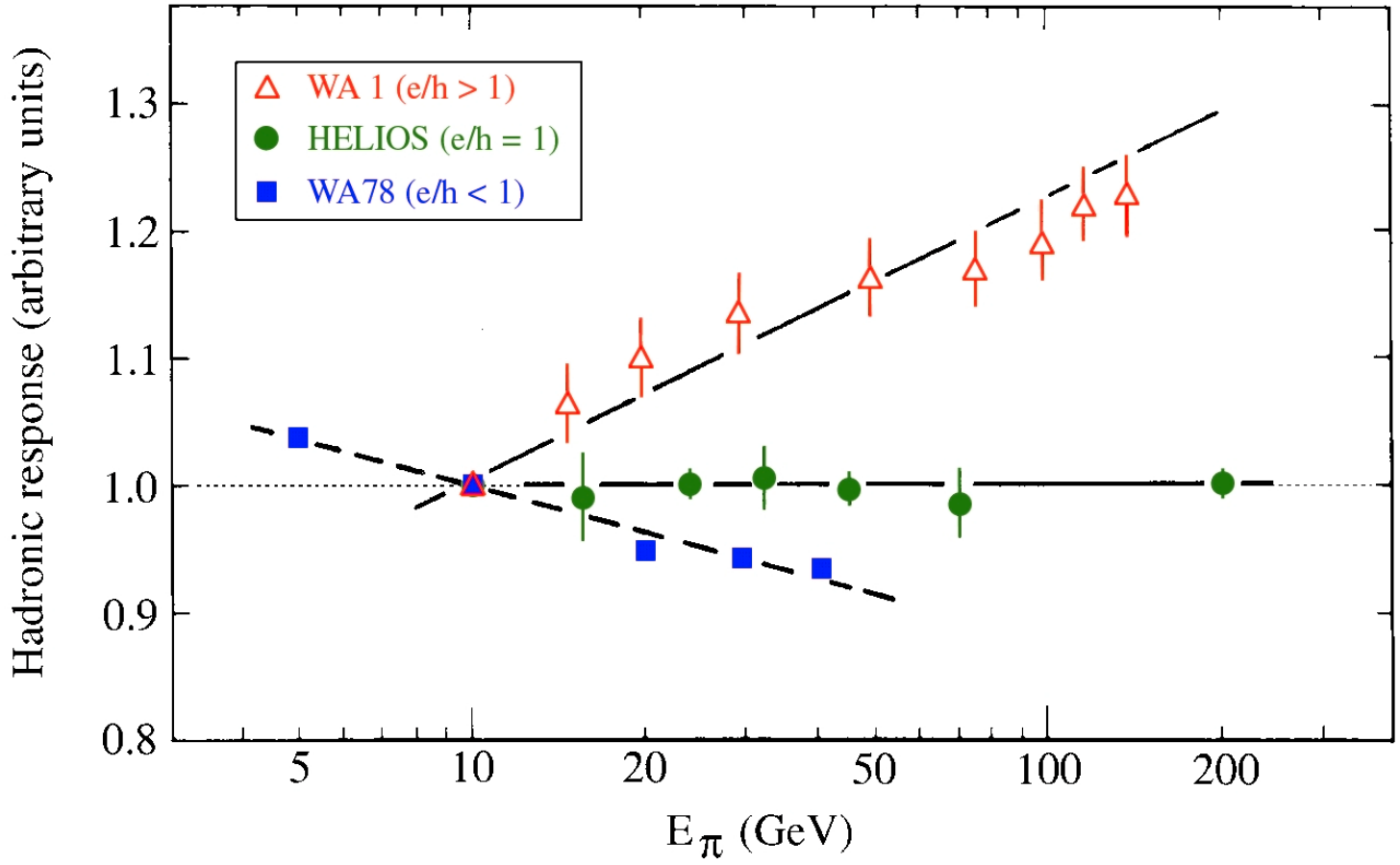

FIG. 3.14. The response to pions as a function of energy for three calorimeters with different e/h values: the WA1 calorimeter ($e/h > 1$, [Abr 81]), the HELIOS calorimeter ($e/h \approx 1$, [Ake 87]) and the WA78 calorimeter ($e/h < 1$, [Dev 86, Cat 87]). All data are normalized to the results for 10 GeV.

Hadronic shower profiles (1)

- Shower profiles are governed by the

  nuclear interaction length, $\lambda_{\rm int}$

  $\lambda_{\rm int}({\rm g\ cm^{-2}}) \propto A^{1/3}$

  $\rightarrow$ Fe 16.8 cm, Cu 15.1 cm, Pb 17 cm, U 10 cm

Hadronic shower profile (longitudinal)

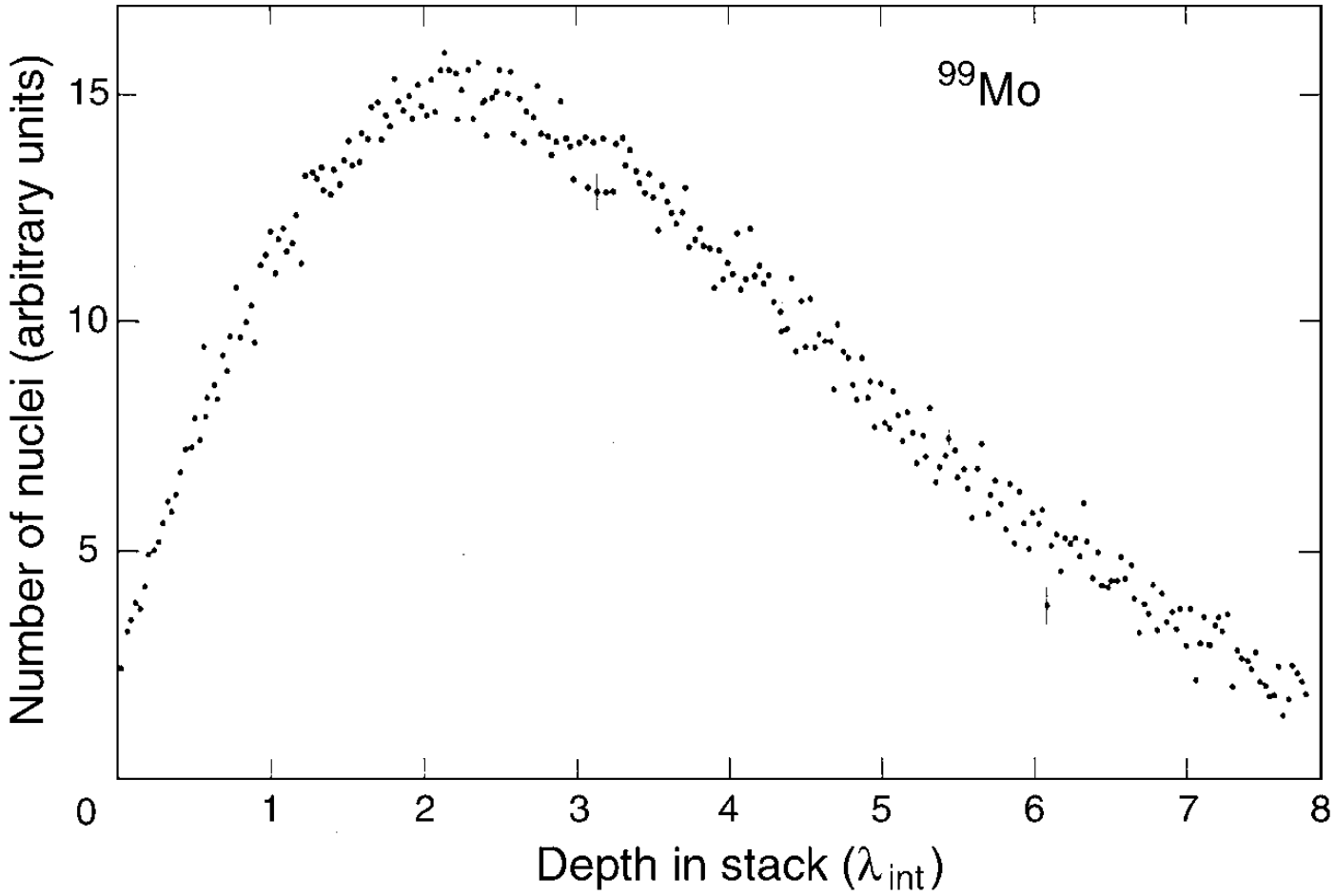

FIG. 2.31. Longitudinal shower profile for 300 GeV π^- interactions in a block of uranium, measured from the induced radioactivity. The ordinate indicates the number of radioactive decays of a particular nuclide, ^{99}Mo, produced in the absorption of the high-energy pions. Data from [Ler 86].

Hadronic shower profiles: Fluctuations!

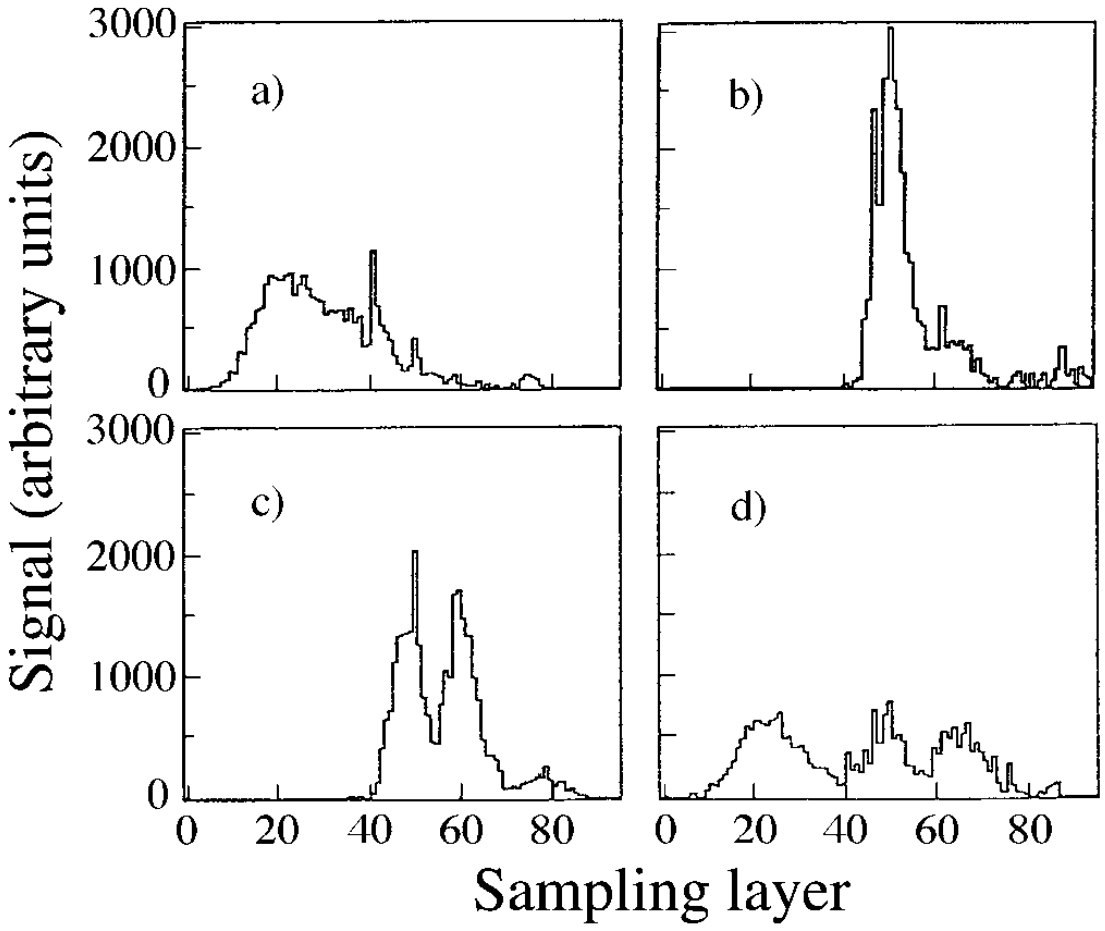

FIG. 2.35. Longitudinal profiles for 4 different showers induced by 270 GeV pions in a lead/iron/plastic-scintillator calorimeter. Data from [Gre 94].

Hadronic shower profiles (2)

- *Lateral* shower profile has two components:
  - *Electromagnetic core* (π^0)
  - *Non-em halo* (mainly non-relativistic shower particles)

Spectacular consequences for *Čerenkov calorimetry*

Čerenkov light is emitted by particles with $\beta > 1/n$

e.g. quartz ($n = 1.45$): Threshold 0.2 MeV for e, 400 MeV for p

Hadronic shower profile (lateral)

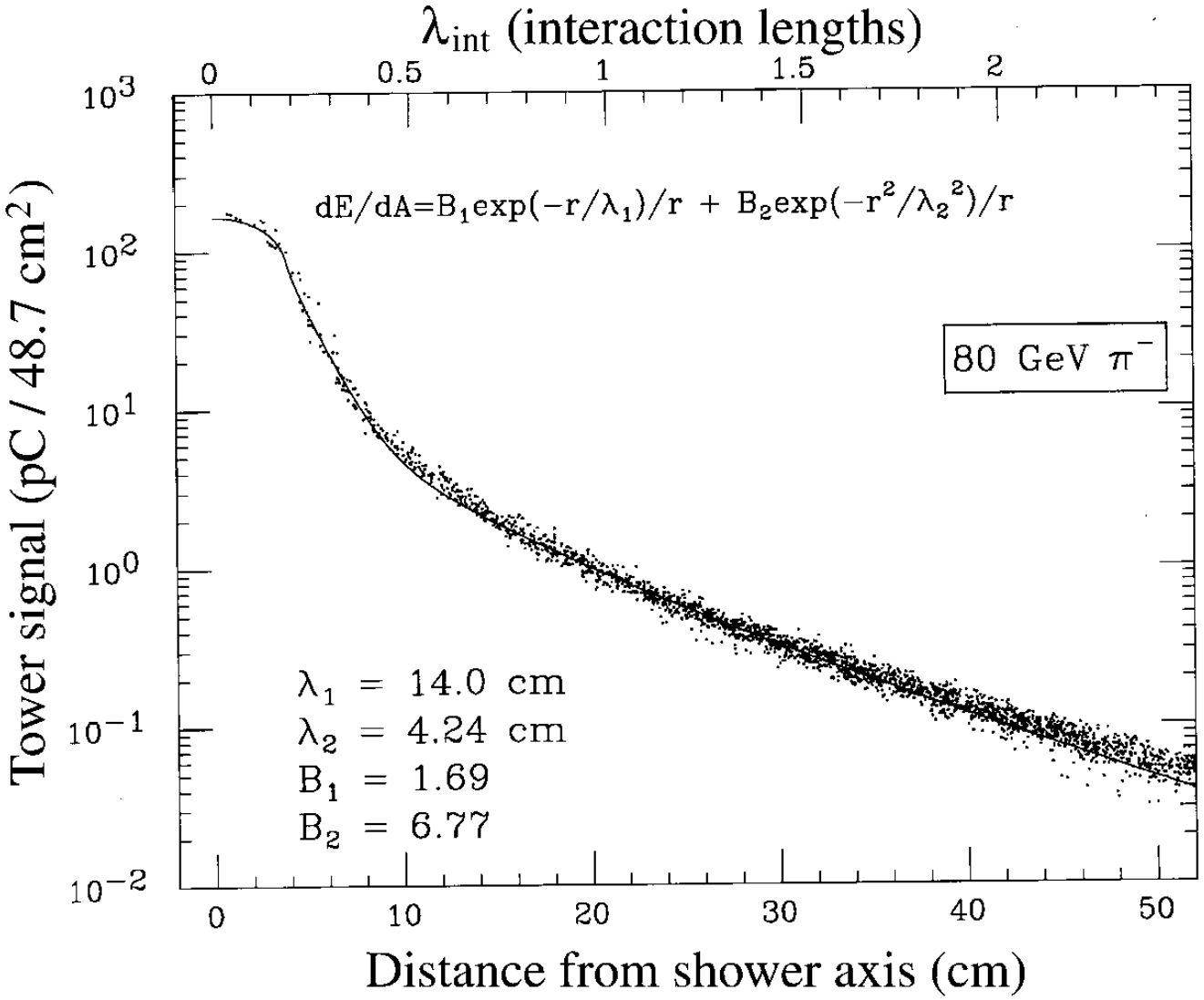

FIG. 2.32. Average lateral profile of the energy deposited by 80 GeV π^-showering in the SPACAL detector. The collected light per unit volume is plotted as a function of the radial distance to the impact point. Data from [Aco 92b].

Nonrelativistic particles dominate tails hadron showers

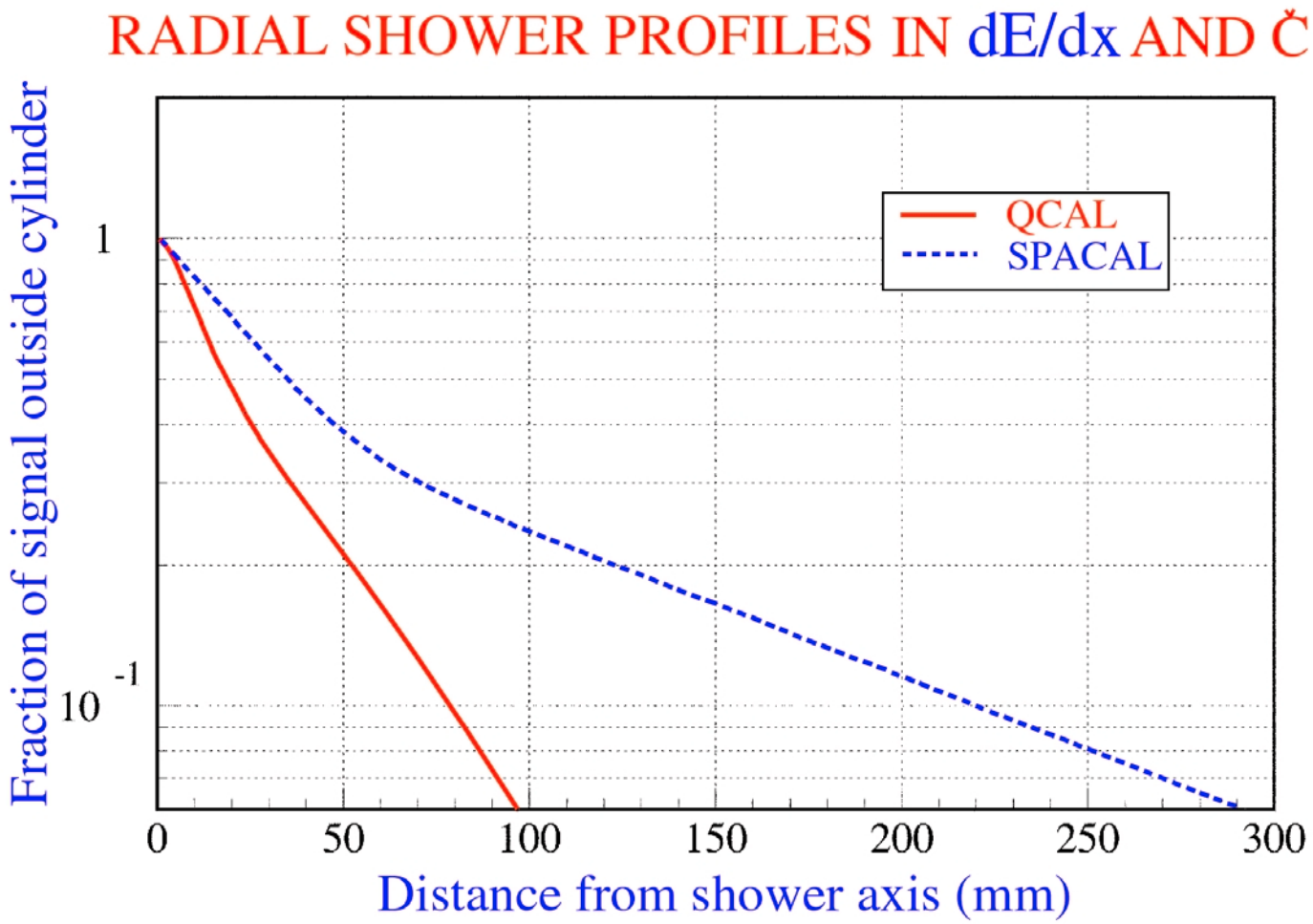

Radial hadron shower profiles (DREAM)

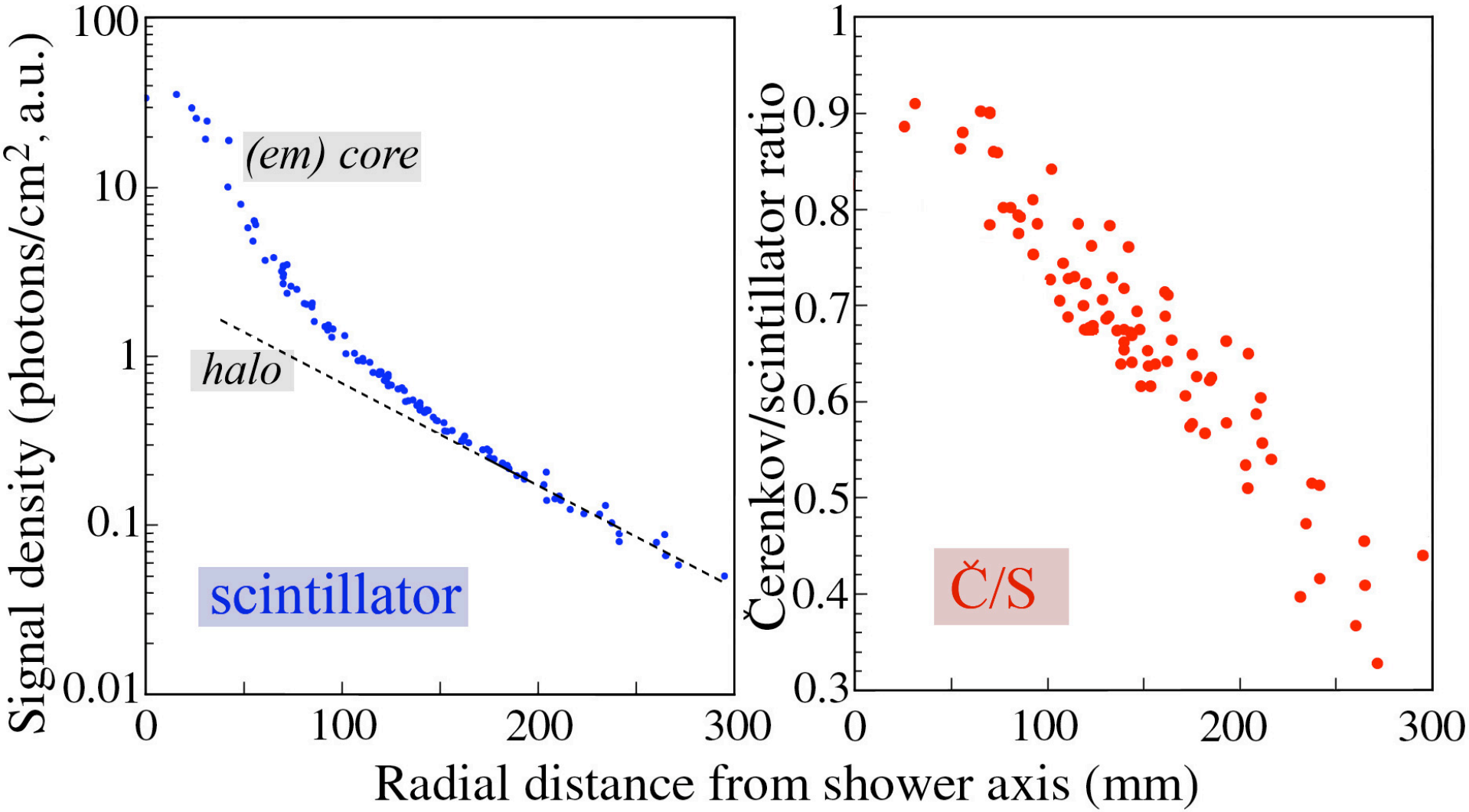

Hadronic shower profiles (3)

- *Shower containment:*
  Depth to contain showers increases with log E
  Lateral leakage *decreases* as the energy goes up!

Hadronic shower leakage (longitudinal)

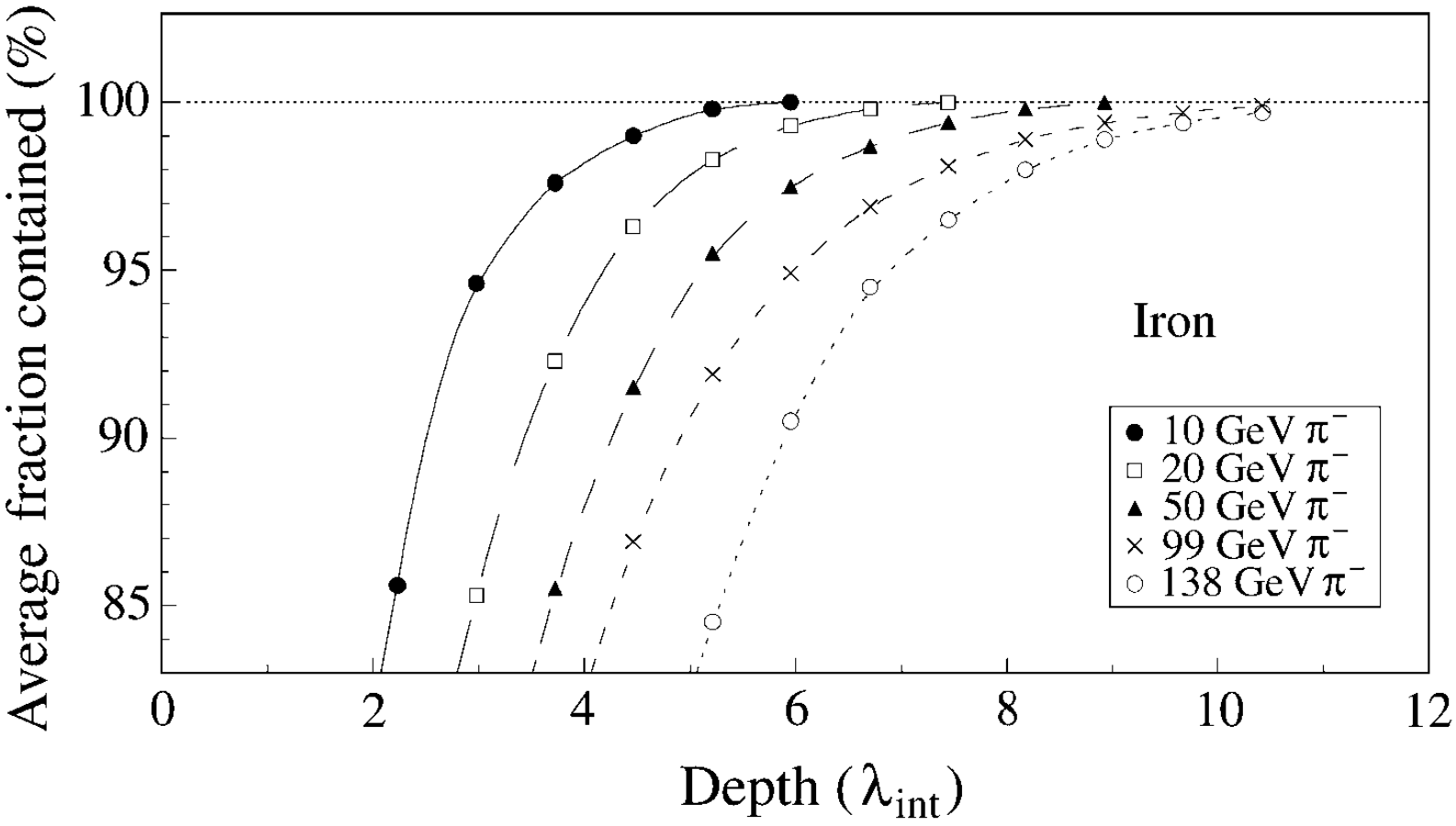

FIG. 2.37. Average energy fraction contained in a block of matter with infinite transverse dimensions, as a function of the thickness of this absorber, expressed in nuclear interaction lengths. Shown are results for showers induced by pions of various energies in iron absorber [Abr 81].

Hadronic shower leakage (lateral)

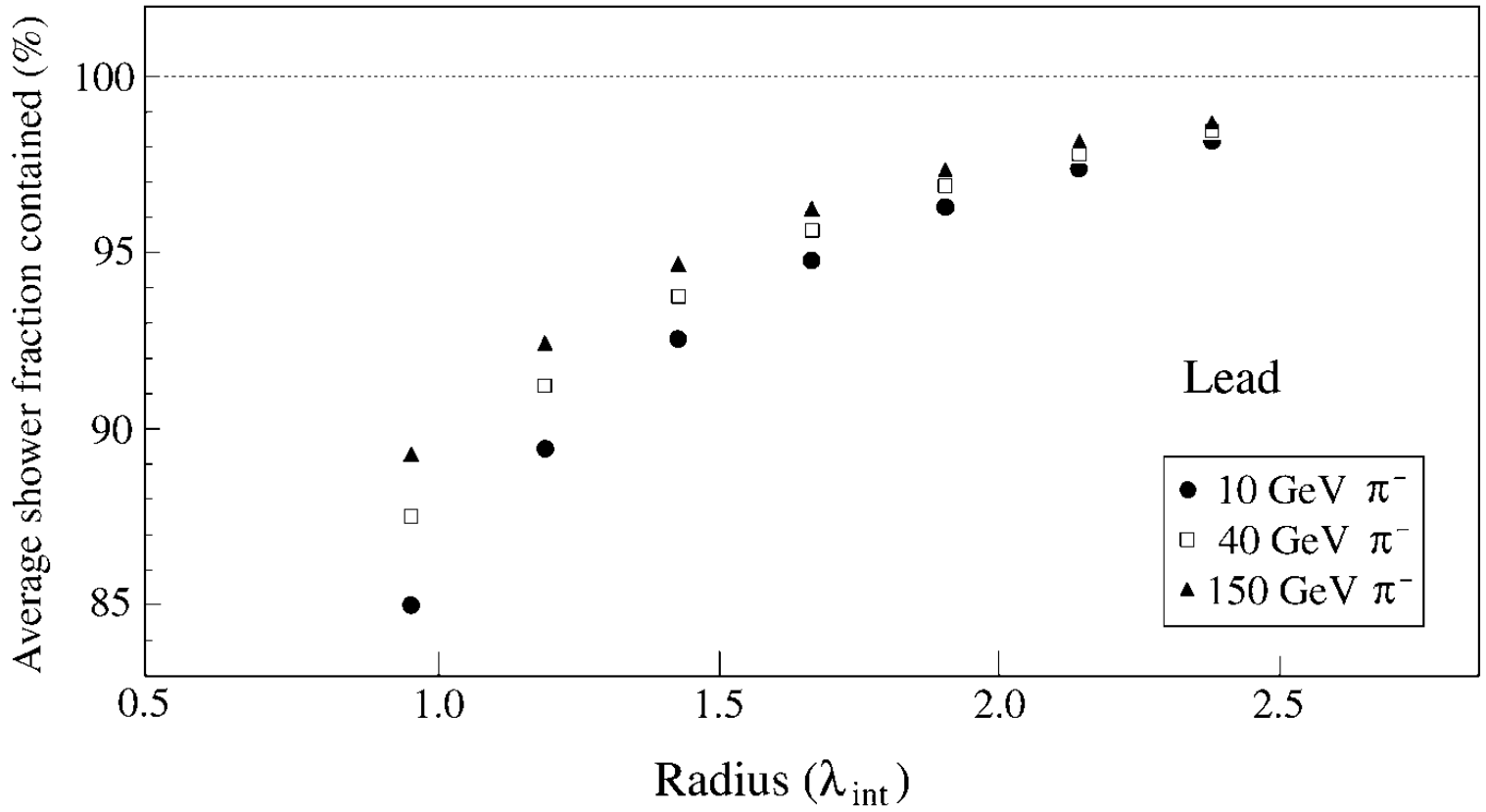

FIG. 2.38. Average energy fraction contained in an infinitely long cylinder of absorber material, as a function of the radius of this cylinder (expressed in nuclear interaction lengths), for pions of different energy showering in lead absorber [Aco 92b].

Hadronic shower profiles (4)

- The $\lambda_{\rm int}/X_0$ ratio is important for *particle ID*
  In high-Z materials: $\lambda_{\rm int}/X_0 \sim 30 \rightarrow$ excellent e/π separator
  1 cm Pb + scintillator plate makes a spectacular *preshower detector*

Comparison of em / hadronic calorimeter properties

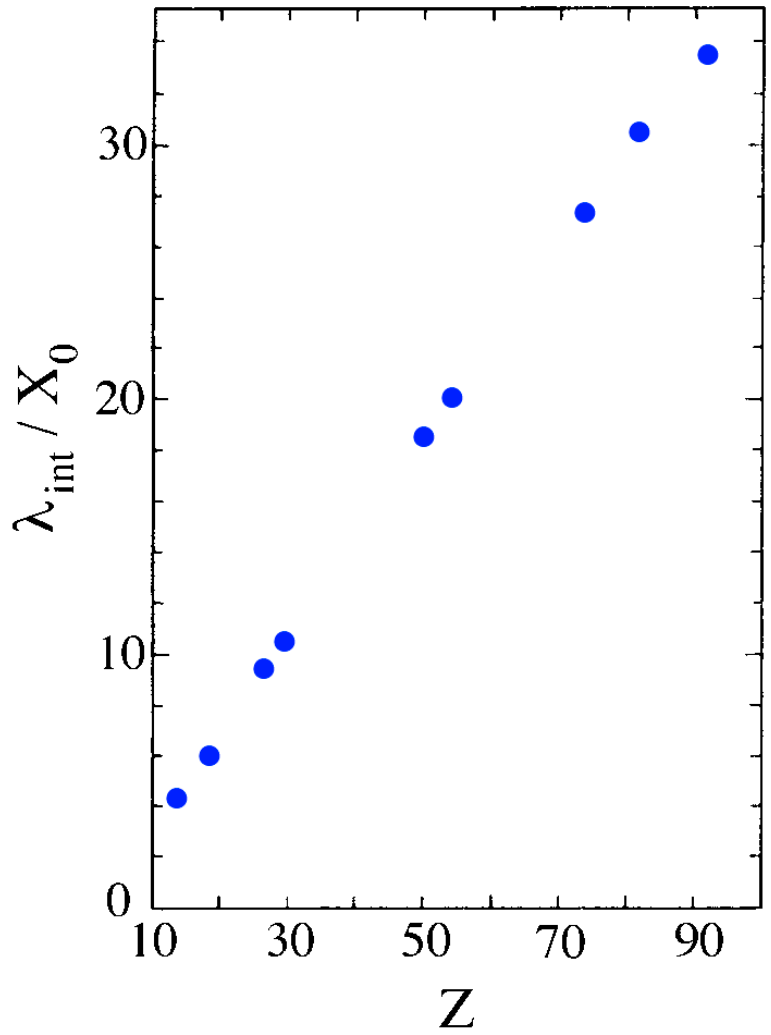

FIG. 7.28. Ratio of the nuclear interaction length and the radiation length as a function of Z.

Particle ID with a very simple Preshower Detector

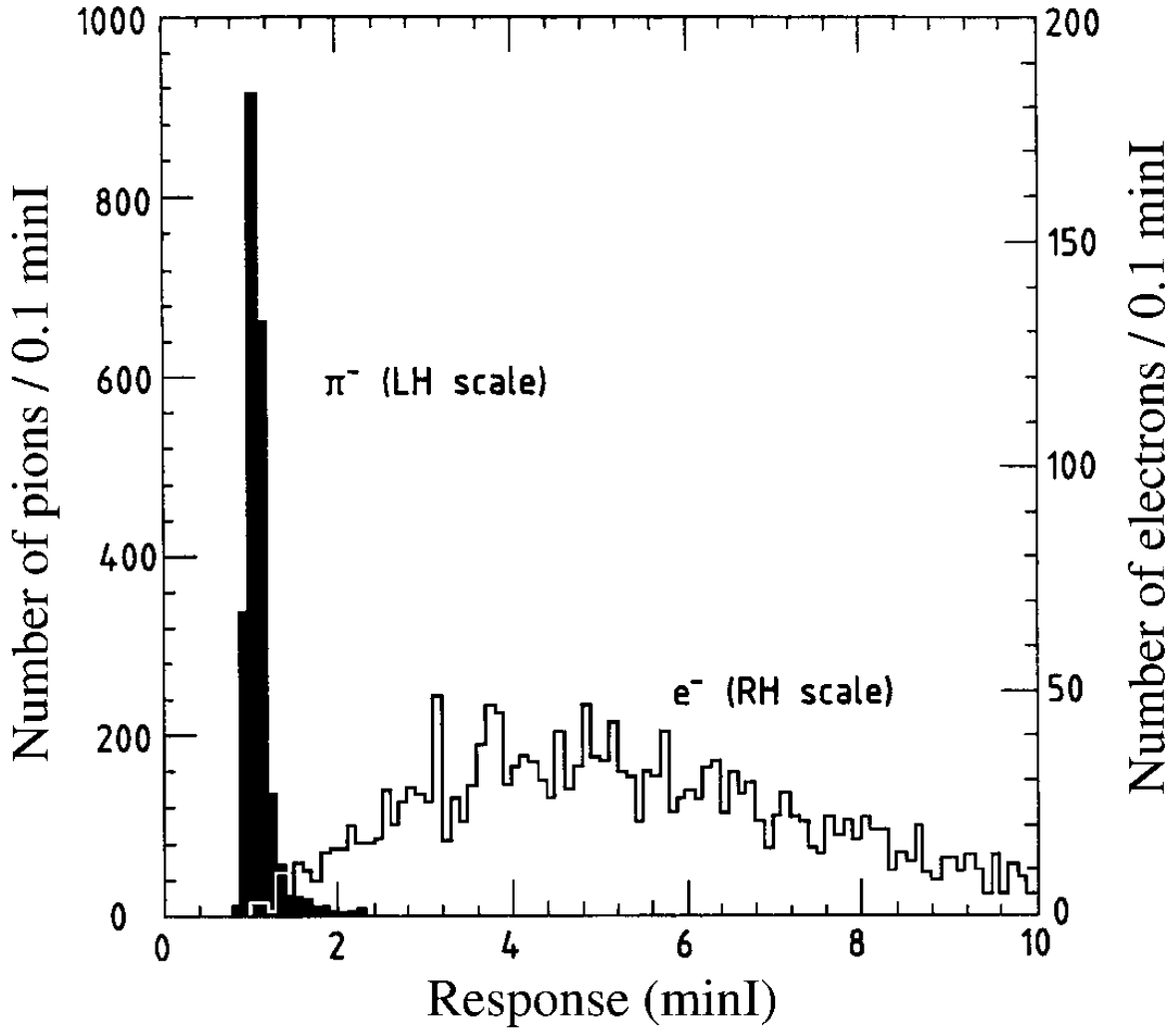

FIG. 7.35. Signal distributions for 75 GeV pions and electrons in a preshower detector used in beam tests of CDF calorimeters.

Lessons for Calorimetry

- In absorption process, most of the energy is deposited by ***very soft shower particles***

- ***Electromagnetic showers:***

  - 3/4 of the energy deposited by e^-, 1/2 by Compton, photoelectrons
    These are *isotropic*, have forgotten direction of incoming particle
    ➡ *No need for sandwich geometry*

  - The typical shower particle is a 1 MeV electron , range < 1 mm
    ➡ important consequences for *sampling calorimetry*

- ***Hadron showers:***

  - Typical shower particles are a 50 - 100 MeV proton
    and a 3 MeV evaporation neutron

  - Range of 100 MeV proton is 1 - 2 cm
    Neutrons travel typically several cm
    What they do depends crucially on details of the absorber

Angular distribution of em shower particles

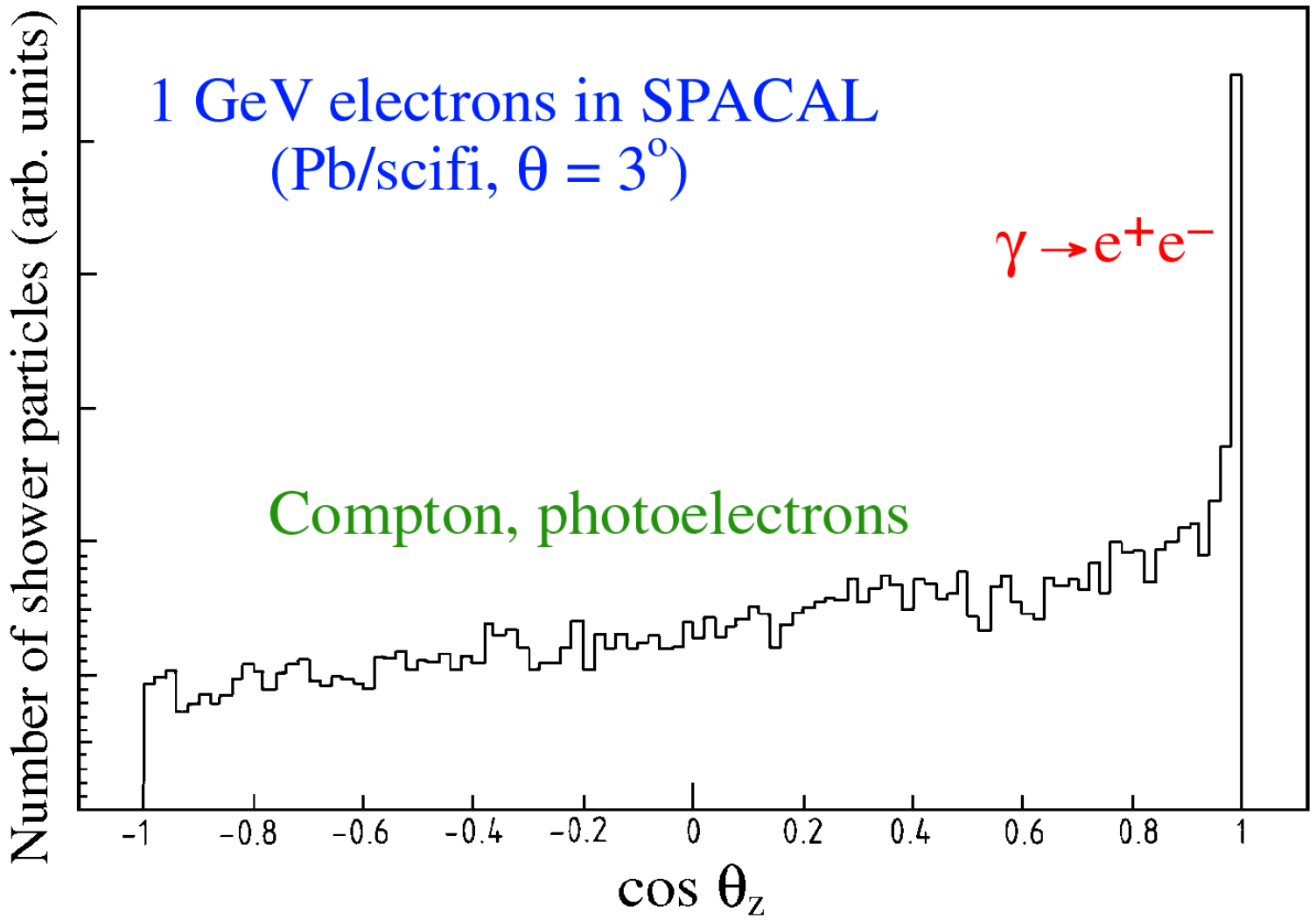

FIG. 2.39. Angular distribution of the shower particles (electrons and positrons) through which the energy of a 1 GeV electron is absorbed in a lead-based calorimeter. Results of EGS4 Monte Carlo simulations. From [Aco 90].

Range of protons generated in hadron showers

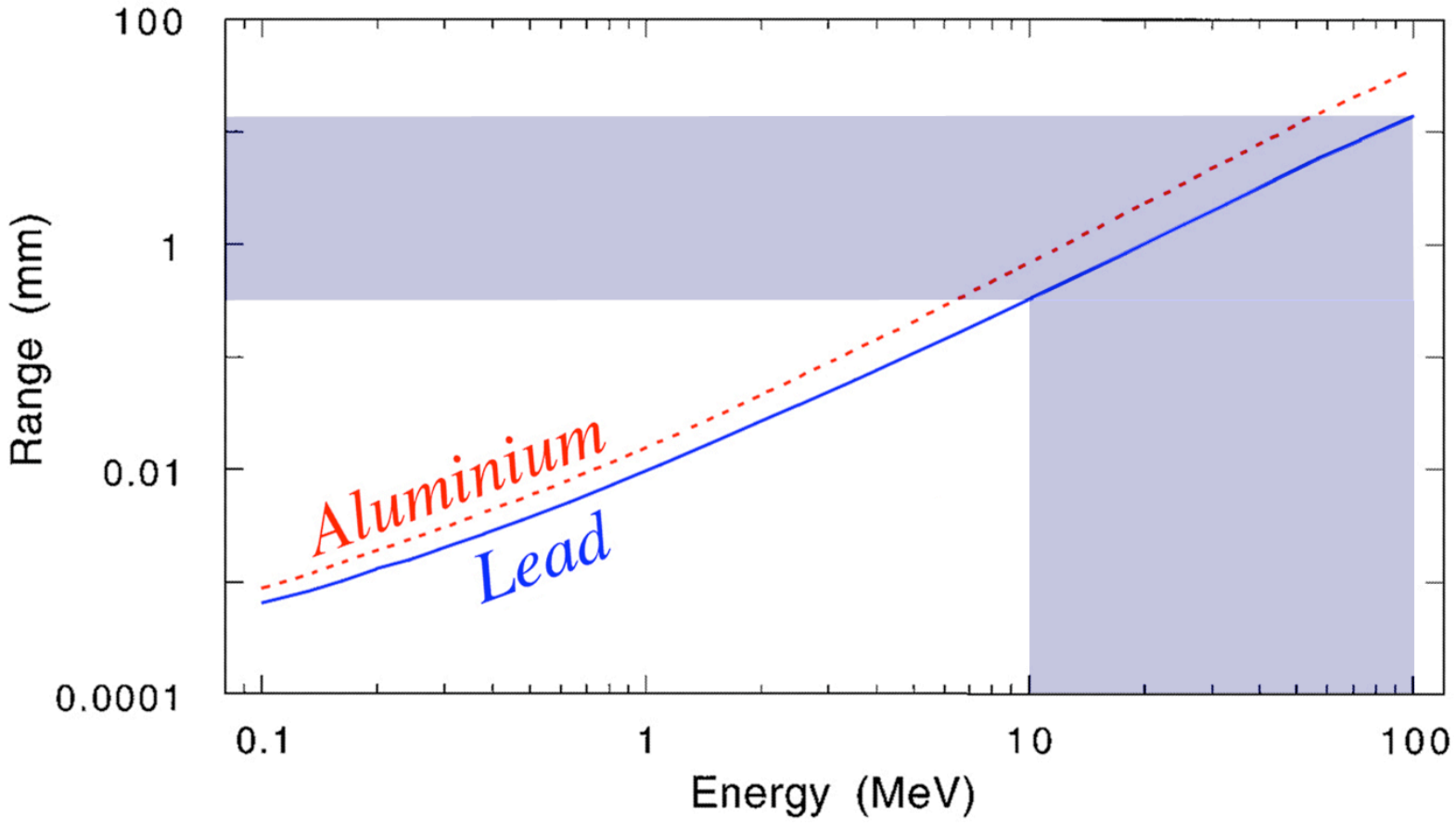

FIG. 2.41. Average range of protons in various absorber materials, as a function of energy [Jan 82].

The Calorimeter Response Function

Response = Average signal per unit of deposited energy

e.g. # photoelectrons/GeV, picoCoulombs/MeV, *etc.*

➡ A *linear* calorimeter has a *constant response*

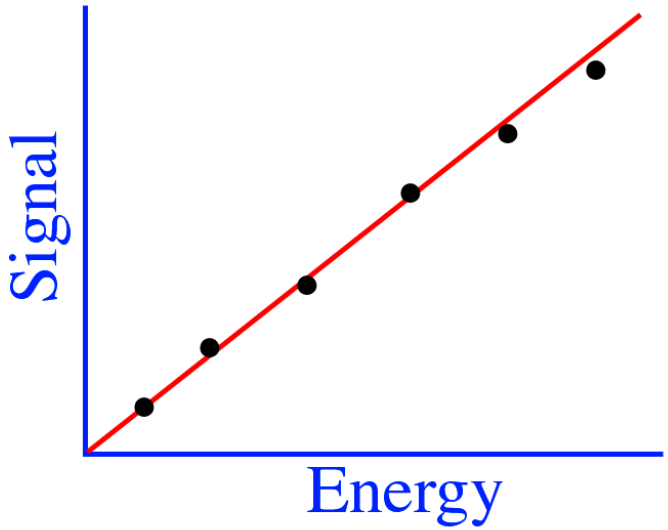

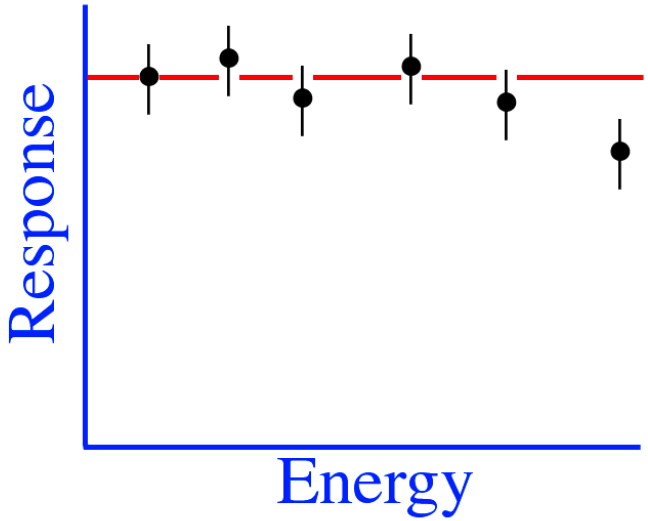

Electromagnetic calorimeters are in general *linear*

All energy deposited through ionization/excitation of absorber

If *not* linear → instrumental effect (saturation, leakage,.....)

Signal linearity for electromagnetic showers

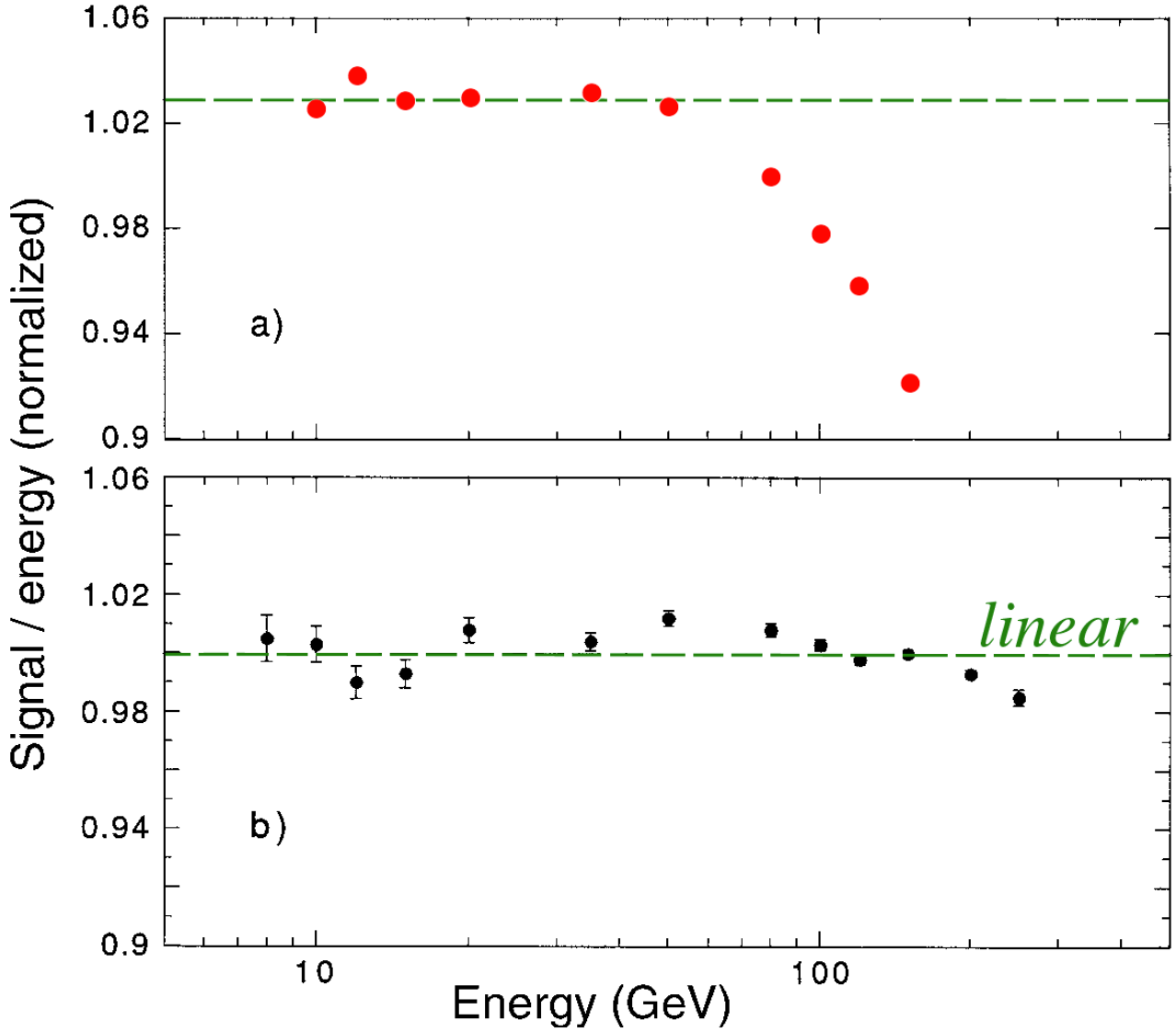

FIG. 3.1. The em calorimeter response as a function of energy, measured with the QFCAL calorimeter, before (a) and after (b) precautions were taken against PMT saturation effects. Data from [Akc 97].

Saturation in "digital" calorimeters (wire chamber readout)

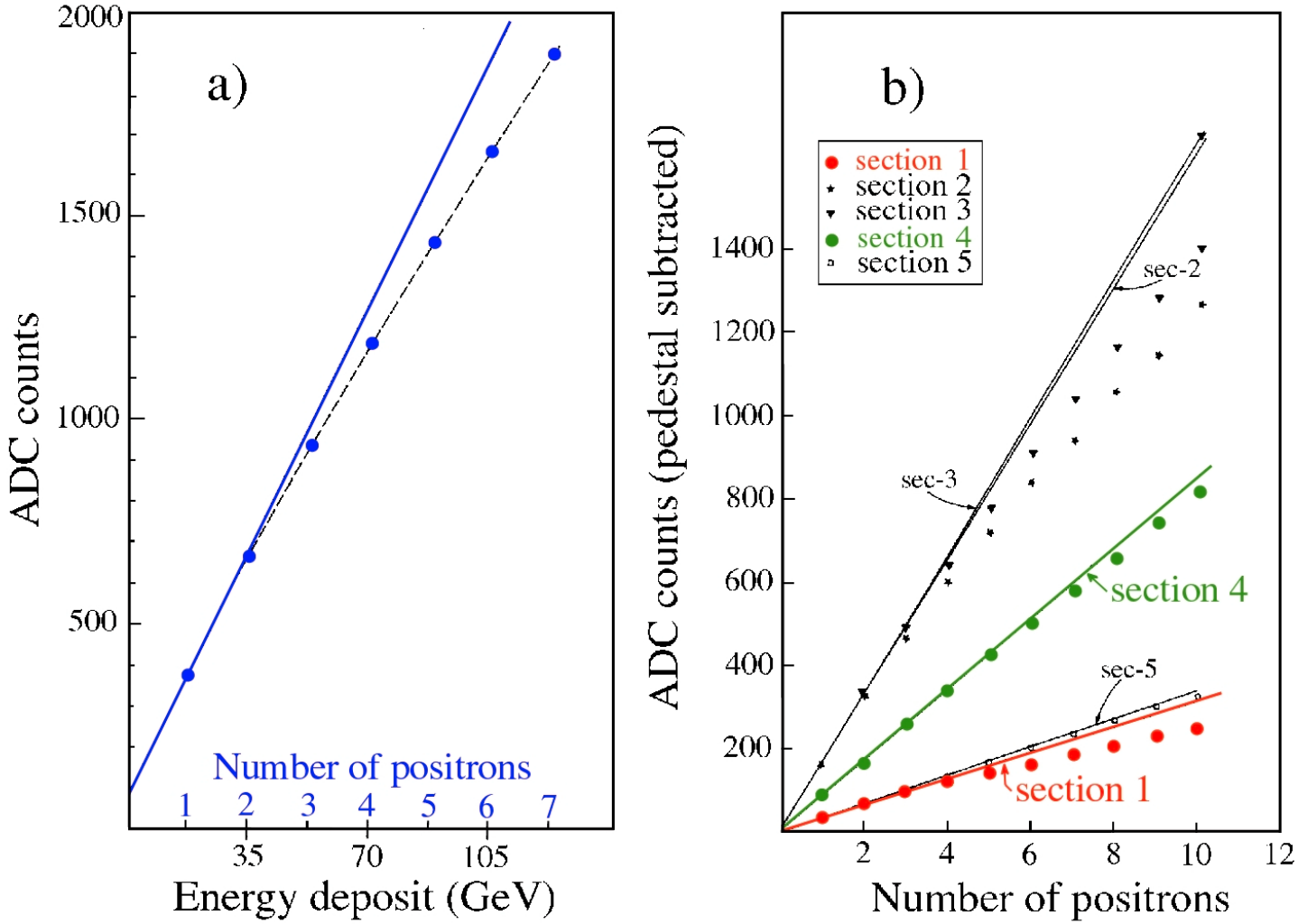

FIG. 3.2. Average em shower signal from a calorimeter read out with gas chambers operating in a "saturated avalanche" mode, as a function of energy. From: NIM 205 (1983) 113.

Fluctuations due to instrumental effects (readout)

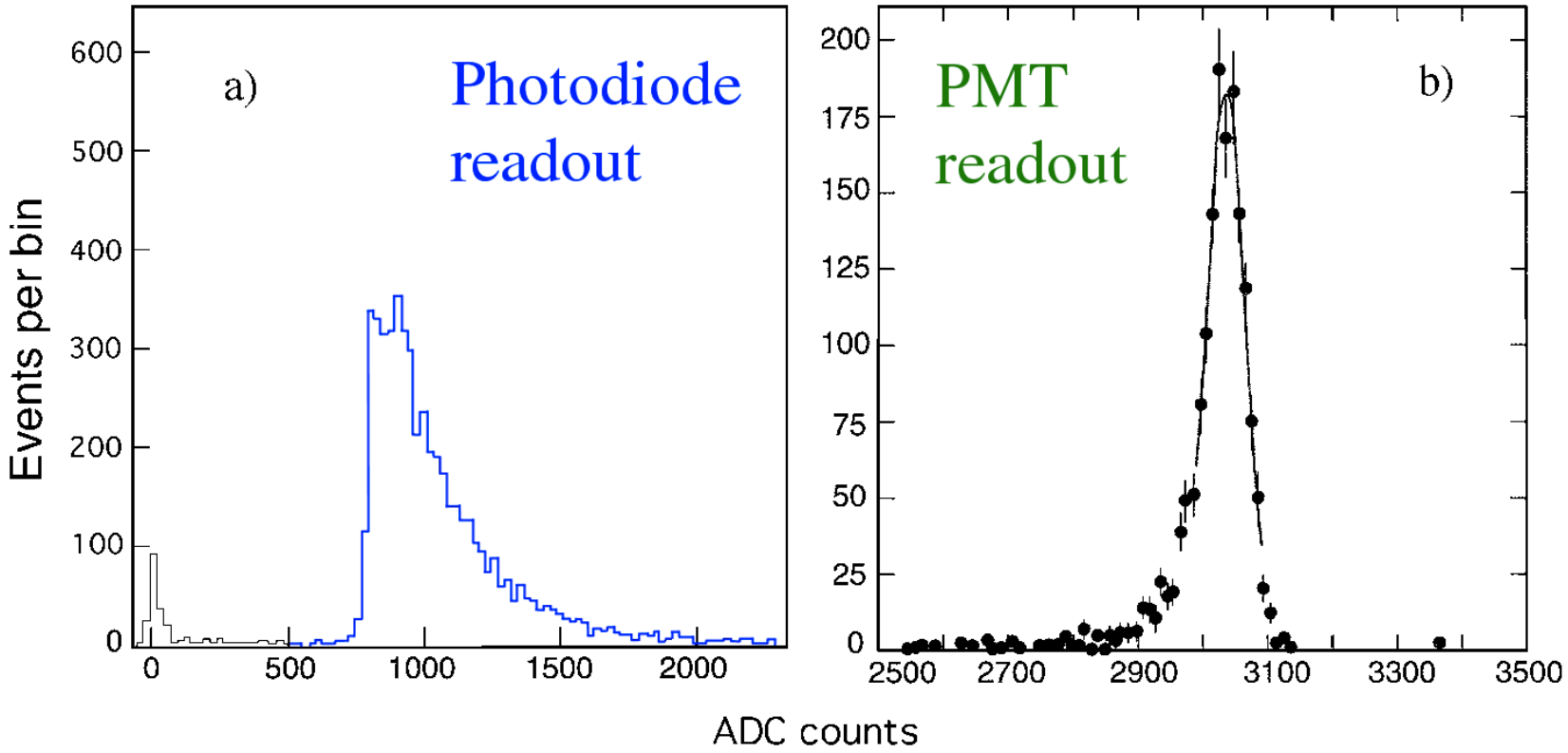

FIG. 3.3. Signal distributions for high-energy electron showers measured with a prototype $PbWO_4$ crystal calorimeter. The calorimeter was read out either with silicon photodiodes (a) or with photomultiplier tubes (b). Data from [Pei 96].

Sampling

- There are *homogeneous* and *sampling* calorimeters
  - Homogeneous: Absorber and active medium are the same
  - Sampling: Only part of shower energy deposited in active medium

$$\textit{Sampling fraction}\ (f_{\text{samp}}) = \frac{\text{energy deposited in active medium}}{\text{total energy deposited in calorimeter}}$$

- f_{samp} is usually determined with a *mip* (dE/dx minimum)

  N.B. *mip*'s do not exist!

  e.g. D0 (em section):

  $3\,\text{mm}\ {}^{238}\text{U}$ $\quad (dE/dx = 61.5\ \text{MeV/layer})$

  $2 \times 2.3\,\text{mm}\ \text{LAr}$ $\quad (dE/dx = 9.8\ \text{MeV/layer})$

  $\Big\}\rightarrow f_{\text{samp}} = 13.7\%$

The *e/mip* ratio

- D0: $f_{\text{samp}} = 13.7\%$
  However, for em showers, sampling faction is only 8.2%
  ➡ *e/mip* ≈ 0.6

- *e/mip* is a function of *shower depth*, in U/Lar it *decreases*
  e/mip increases when the *sampling frequency* becomes very high
  What is going on?

- *Photoelectric effect:* $\sigma \propto Z^5$, $(18/92)^5 = 3 \cdot 10^{-4}$
  $\rightarrow$ Soft γs are very inefficiently sampled
  Effects strongest at high Z, and late in the shower development
  The range of the photoelectrons is typically < 1 mm
  $\rightarrow$ if absorber layers are thin, they may contribute to the signals

Sampling calorimeters: The e/mip signal ratio

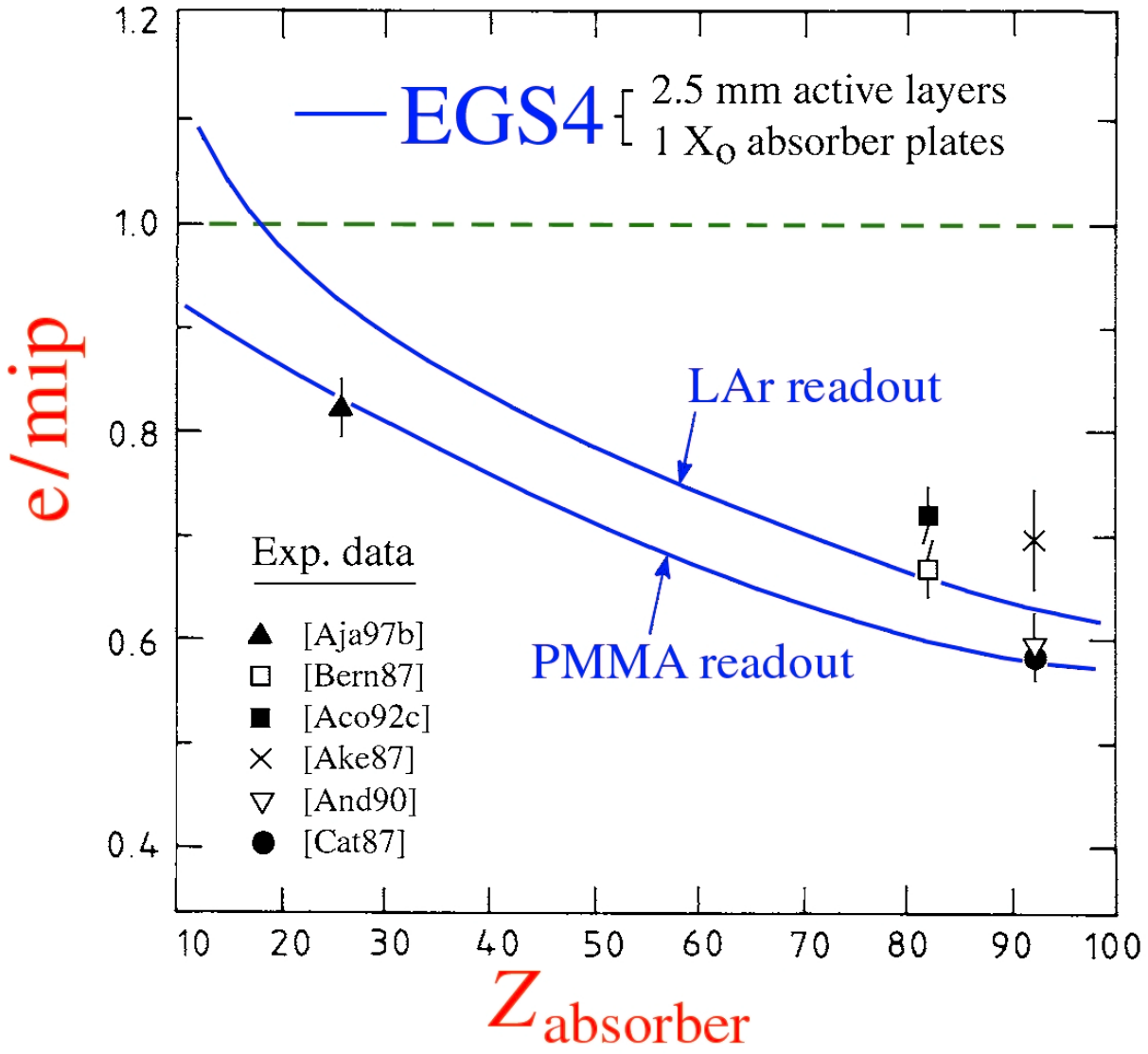

FIG. 3.7. The e/mip ratio for sampling calorimeters as a function of the Z value of the absorber material, for calorimeters with plastic scintillator or liquid argon as active material. Experimental data are compared with results of EGS4 Monte Carlo simulations [Wig 87].

The EM sampling fraction changes with depth!

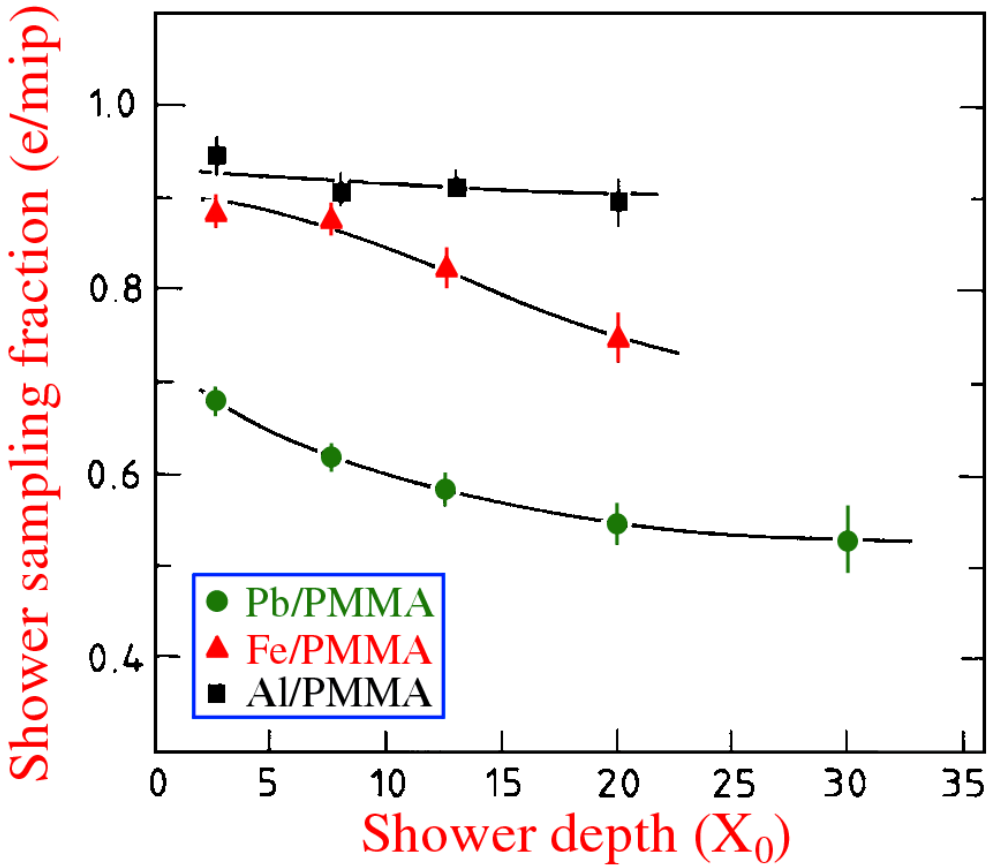

FIG. 3.8. The e/mip ratio as a function of the shower depth, or age, for 1 GeV electrons in various sampling calorimeter configurations. All calorimeters consist of 1 X_0 thick absorber layers, interleaved with 2.5 mm thick PMMA layers. Results from EGS4 Monte Carlo simulations [Wig 87].

The e/mip ratio: Dependence on calorimeter parameters

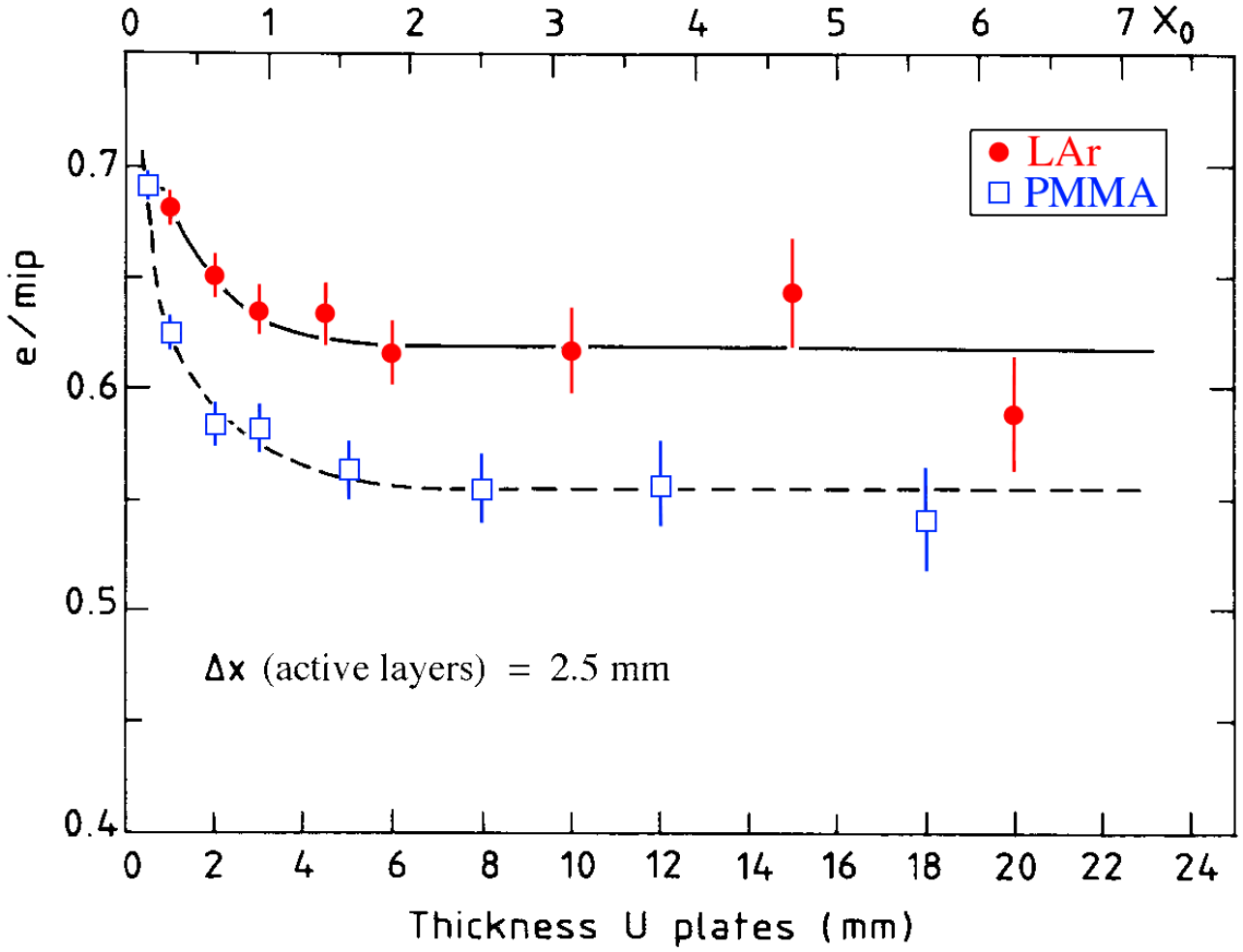

FIG. 3.9. The e/mip ratio as a function of the thickness of the absorber layers, for uranium/PMMA and uranium/LAr calorimeters. The thickness of the active layers is 2.5 mm in all cases. Results from EGS4 Monte Carlo simulations [Wig 87].